Genes to Cells,
2019 年 2 月 発行, 第 24 巻 第 2 号, 126-138 頁

主論文

Article type : Original Article

Nucleus-localized adiponectin is survival gate keeper through miR-214-mediated *AIFM2* regulation

Junkwon Cho[1], Rika Teshigawara[1], Masahiro Kameda[1], Shinpei Yamaguchi[2] and Takashi Tada[1]

[1]*Laboratory of Developmental Epigenome, Department of Regeneration Science and Engineering, Institute for Frontier Life and Medical Sciences, Kyoto University,* [2]*Laboratory of Stem Cell Pathology, Graduate School of Frontier Biosciences, Osaka University*

Short title: Nuclear Adiponectin in Cell Survival

Disclosure Statement: The authors have nothing to disclose.

Key words: Adiponectin, Nuclear localization, Monomer, Cell death, miR-214, *AIFM2*

Correspondence: Takashi Tada

Laboratory of Developmental Epigenome, Department of Regeneration Science and Engineering,

Institute for Frontier Life and Medical Sciences, Kyoto University

This article has been accepted for publication and undergone full peer review but has not been through the copyediting, typesetting, pagination and proofreading process, which may lead to differences between this version and the Version of Record. Please cite this article as doi: 10.1111/gtc.12658

53 Kawahara-cho, Shogo-in, Sakyo-ku, Kyoto 606-8507 JAPAN

Tel: +81-75-751-4102, Fax; +81-75-751-4114

E-mail: ttada@infront.kyoto-u.ac.jp

Abstract

Adiponectin secreted from adipocytes into plasma has anti-aging, anti-obesity, and anti-inflammation effects. Here, we detected intracellular adiponectin localized in the nuclei of human and mouse pluripotent stem cells, mouse germ cells, and some somatic cells. Nucleus-localized (Nu) adiponectin protein is characterized by an N-terminal truncated monomer form in a native state, compared with intact multimer forms of cytoplasm-localized (Cy) adiponectin protein. Doxycycline-induced overexpression of ADIPONECTIN caused cell death in human and mouse Nu-type pluripotent stem cells. Genome-wide gene expression analysis indicated that apoptosis by ADIPONECTIN overexpression was induced in accompany with upregulation of *AIFM2* and *MEG3*. Upregulation of *AIFM2* and *MEG3* and downregulation of miR-214-3p verified by qPCR analyses after ADIPONECTIN overexpression indicated that the MEG3-miR-214-AIFM2 pathway played a role in the apoptotic cell death of pluripotent cells. Adiponectin-induced cell death was rescued by the treatment with miR-214-3p mimic. Global data analysis demonstrate that Nu adiponectin has a role in

microRNA-mediated post-transcription regulation, cell-cell interactions, and chromatin remodeling as a survival gate keeper.

1 | INTRODUCTION

Adipose tissue is an endocrine organ that produces bioactive proteins known as adipokines. Adiponectin (APN/Apn) is an important 28-30 kDa collagen-like hormone belonging to the C1q/TNF superfamily encoded by the *ADIPONECTIN*/*Adiponectin* (*APN/Apn*) (also known as *Adipoq*, *Acrp30*, *apM1*, and *GBP28*) gene, which spans 17 kb on human chromosomal locus 3q27 and contains three exons (Shapiro & Scherer, 1998). APN/Apn protein contains 244 amino acids (aa) in humans and 247 aa in mice and consists of four structural domains: a C-terminal globular domain homologous to C1q, a collagenous domain of 22 G-X-Y repeats, a hyper-variable region, and an N-terminal signal peptide (Sherer, Williams, Fogliano, Baldini, & Lodish, 1995). The C1q domain is highly conserved between humans and mice. Adipose adiponectin in a native state is highly polymerized, and has a low molecular weight form (LMW, 3 mers), a middle molecular weight form (MMW, 6 mers), or a high molecular weight form (HMW, 12-18 mers).

APN/Apn is abundantly secreted from adipose tissue, but a low level of expression is observed in other tissues including colonic mucosa, liver, skeletal muscle, placenta, salivary glands, bone, myocytes, and myofibroblasts (Sun, et al. 2009). Apn levels have strong sexual dimorphism; females average twice the levels of males because of testosterone (Combs, et al. 2004). A number of APN/Apn receptors, AdipoR1, AdipoR2, and T-cadherin, have been identified (Yamauchi et al., 2003a; Hug et al., 2004). AdipoR1 expression is ubiquitous, whereas AdipoR2 expression is tissue specific to the liver irrespective of integral membrane proteins with highly similar sequences. Plasma APN/Apn exerts receptor-mediated anti-aging effects on several tissues such as the liver, heart, pancreatic beta cells, kidney, muscle, and in many other cell types.

Plasma APN/Apn has pleiotropic functions in many tissues and conditions. APN/Apn suppresses hepatic gluconeogenesis, promotes insulin sensitization, and improves whole body energy homeostasis (Achari & Jain 2017). Imbalanced production of APN/Apn contributes to the pathogenesis of obesity-linked metabolic and cardiovascular diseases. Obesity-linked metabolic diseases are associated with a number of pathological events by inhibiting inflammation, suppressing cell death, and enhancing cell survival.

To explore Apn loss-of-function, Apn-deficient mice were generated by deletion of all three *exons* and the 5'-untranslated region of *Apn* (Nawrocki et al., 2006), deletion of *exon* 2 and 3 of *Apn*

(Kubota et al., 2002), or deletion of only *exon* 2 (Maeda et al., 2002). All mice were viable and fertile, which demonstrates that Apn is dispensable for normal development. However, Apn-null mice develop metabolic syndromes including obesity, hyperglycemia, hypertension (Ouchi et al., 2003), liver fibrosis and injury (Matsumoto et al., 2006), heart defects (Liao et al., 2005), and kidney defects (Jin, Chen, Hu, Chan, & Wang, 2013). Plasma Apn maintains normal metabolism by controlling obesity-related events.

To explore Apn gain-of-function, tissue-specific and ubiquitous overexpression of *Apn* was examined using transgenic (Tg) mouse lines. For tissue-specific overexpression, exogenous *Apn* driven by the adipose-specific enhancer/promoter of the *aP2* gene delivered moderate levels of excess expression in Tg mice (aP2-Apn Tg mice) (Combs et al., 2004). The aP2-Apn Tg mice exhibited unusual features including expansion of the interscapular region and bilateral exophthalmia (Combs et al., 2004), an autologous regulatory feedback loop in Apn regulation (Bauche et al., 2006), and impaired adipocyte differentiation (Bauche et al., 2007). Another tissue-specific promoter used for making Apn Tg mice was the human serum amyloid P (SAP) specific to the liver (SAP-Apn Tg mice). SAP-Apn Tg mice exhibited altered protection against atherosclerosis (Yamauchi et al., 2003b) and prevention of premature death by a high-calorie diet (Otabe et al., 2007). Ubiquitous overexpression of Apn in Tg mice using the cytomegalovirus (CMV) minimal promoter (CMV-Apn

Tg mice) were produced, but could not be established as a Tg line because of fertility problems (Combs et al., 2004). In mice, an increase in plasma Apn is inversely associated with obesity and insulin-resistance, which significantly prolongs life span *in vivo* (Otabe et al., 2007). However, it is unclear why mortality or sterility occur in Tg mice ubiquitously overexpressing Apn based on the known functions of plasma Apn.

In this study, we found that Doxycycline (Dox)-inducible overexpressed APN/Apn resulted in cell death in human intermediately reprogrammed stem (iRS) and mouse embryonic stem (ES) cells in which APN/Apn accumulated in the nucleus. Nucleus-localized (Nu) APN/Apn was characterized by a monomer form in iRS/ES cells in contrast with multimer forms of cytoplasm-localized (Cy) APN/Apn in adipocytes. Monomer Nu APN/Apn was the N-terminal-truncated form. Expression microarray analysis revealed expression changes of caspase-independent but not dependent genes by Dox-inducible APN overexpression. Comparative qPCR analyses between Dox (-) and Dox (+) iRS cells revealed significant upregulation of *AIFM2* (*apoptosis-inducing factor, mitochondrion-associated 2*) and *MEG3* (*maternally expressed gene 3*) and downregulation of miR-214-3p, which are involved in caspase-independent apoptosis in association with APN overexpression. Adiponectin overexpression-induced cell death was rescued by the treatment with miR-214-3p mimic in company with downregulation of *AIFM2* expression. Nu APN/Apn likely

controls cell survival through microRNA-mediated post-transcription regulation, cell-cell interactions, and chromatin remodeling.

2 | RESULTS

2.1 | Nuclear localization of Apn in somatic and germ cells

Apn is an adipokine abundantly secreted from adipose tissue, but low expression of Apn is observed in other tissues (Sun et al., 2009). Expression of Apn protein was detected in all tissues examined by immunostaining with an antibody recognizing the globular domain of Apn (Ct1) (Fig. 1A). Positive Apn antibody signals were found in the nucleus and cytoplasm of primary cultured cells from the heart, lung, and tail tip, in contrast with their cytoplasmic localization in pre-adipocytes. To examine whether Apn was expressed in germ cells, male and female primordial germ cells (PGCs) collected from 12.5 *dpc* embryos of Oct4-GFP transgenic mice were immunostained. Male somatic nuclei and female early meiotic nuclei were all positive for Apn (Fig. 1B). These data demonstrated that a low level of Apn was localized in the nucleus or cytoplasm of somatic and germ cells compared with adipose cells in which highly expressed Apn accumulated in the cytoplasm. Expression of mouse

Apn in adipocytes is several hundreds to a thousand times higher than expression of Apn in other cells (GEO accession number: GSE10246).

2.2 | Inducible overexpression of APN in mouse embryonic fibroblasts

To examine Nu and Cy Apn in mouse embryonic fibroblasts (MEFs), heterogeneous primary cultured cells from 12.5 *dpc* embryos were immunostained with anti-Apn antibody (Ct1) (Fig. 2A). Some MEFs had a Nu-type, and others had a Cy-type. Approximately equal numbers of Nu (52%) and Cy-type (48%) cells were observed. We were unable to clarify which cell type exhibited the Nu pattern.

To explore the effects of differentially localized Apn, the Dox-inducible human *APN* gene was introduced into MEFs by lentivirus-mediated transduction (Fig. 2B, upper). Overexpression of human APN was detected by the signal intensity of immuno-reaction with the Ct1 antibody in Dox (+) compared with Dox (-) (Fig. 2B, left panels). Selective cell loss was observed 48 hours after Dox (1 μg/mL) treatment (Fig. 2B, right). Cell death was significantly higher in MEFs with Dox than in those without Dox. The number of Nu-type cells decreased from 91% to Cy-type in Dox (-) to 42% to Cy-type in Dox (+). No harmful effect of the presence of Dox in culture at the concentration of 2.0

μg/mL on cell proliferation was detected (Supplementary material Fig. S1). Therefore, the detrimental effects of overexpressed APN on survival were more obvious in Nu-type cells than in Cy-type cells.

2.3 | Nuclear localization of Apn in mouse ES cells

To explore clonal cell lines exhibiting nuclear localization of Apn, mouse ES cells, which are blastocyst-derived pluripotent stem cells, were examined. *Apn* transcription was detected by RT-PCR in mouse ES cells (Fig. 3A). Immunostaining with the Ct1 antibody demonstrated that Apn protein was localized in the nuclei of ES cells as the Nu-type Apn (Fig. 3A). Localization of Apn in ES cell nuclei was verified with another anti-APN/Apn antibody (Ct2) recognizing the C-terminal globular domain (Fig. 1A; Supplementary material Fig. S2). Western blot analyses with the Ct1 antibody in a native state (non-reduced) revealed a 30-kDa band with protein from ES cells (Dox (-)), regardless of higher molecular bands of multimer protein complexes from adipose tissue as previously reported (Schraw, Wang, Halberg, Howkins, & Scherer, 2008) (Fig. 3B). Apn protein in ES cell nuclei was in a monomer protein form in contrast with the multimer forms in the cytoplasm of adipose tissue. Nuclear localization of Apn protein was reconfirmed by western blot hybridization analyses with ES cell protein separated from the nucleus and cytoplasm (Fig. 3B).

2.4| Inducible overexpression of APN in mouse ES cells

To produce a Dox-inducible human *APN* overexpression system, a single plasmid containing the regulatory and operator elements in which the PGK promoter-driven *APN* gene was Dox-dependently activated (Fig. 3C, upper) was electroporated into mouse ES cells. First, clones resistant to puromycin treatment were expanded as candidate clones. Second, positive clones were selected based on the response to Dox treatment. Increases in *APN* expression were Dox dose-dependent (Fig. 3C, middle). Consistent with the RT-PCR analysis, a Dox-inducible increase in APN protein was detected by western blot hybridization (Fig. 3B).

To investigate the effects of APN overexpression on Nu-type ES cells, the number of surviving cells was compared between cultures with or without Dox. Cells were sub-cultured for 12 hours after the beginning of Dox treatment. The number of surviving cells decreased significantly 24-36 hours after Dox administration (Fig. 3C, lower). The viability and pluripotency of surviving ES cells were analyzed by alkaline phosphatase staining (Fig. 3D). The number of alkaline phosphatase-positive cells was significantly decreased as a consequence of overexpression of APN induced by Dox treatment.

2.5 | Nuclear localization of APN in human pluripotent stem cells

To investigate the effects of APN overexpression in human cells, APN expression and protein localization were examined in iPS cells and iRS cells, which are pre-iPS cells capable of resuming reprogramming processes into iPS cells by responding to stimuli given by changes in culture conditions (Teshigawara, Hirano, Nagata, Ainscough, & Tada, 2016). The iRS cell clones are uniformly DsRed positive, and iRS cell-derived iPS cell clones are DsRed negative (Teshigawara et al., 2016). Transcription of endogenous *APN* was detected by RT-PCR analysis in iPS and iRS cells (Fig. 4A). Immunostaining with an anti-Apn antibody (Ct1) demonstrated the nuclear localization of APN protein in iPS and iRS cells (Fig. 4A). Localization of APN in iRS cell nuclei was verified with another anti-APN/Apn antibody (Ct2) recognizing the C-terminal globular domain (Fig. 1A; Supplementary material Fig. S2). Human iRS cells were suitable for survival assay in this study, because of difficulties in single cell cloning of human iPS cells, and the higher survival rate of iRS cells than that of iPS cells through subculture. Western blot hybridization analysis revealed that, as with mouse Apn, human APN existed as a monomer under a native condition (Fig. 4B). Nuclear localization of APN protein was confirmed by western blot hybridization analyses with the nucleus and cytoplasm protein separated from whole protein of iRS cells (Fig. 4B).

2.6 | Inducible overexpression of APN in human iRS cells

The same construct used for mouse ES cells (Fig. 3C, upper) was introduced by electroporation into iRS cells. After drug selection with puromycin, clones responsive to Dox treatment were selected as positive. A dose-dependent Dox increase in human *APN* was confirmed by RT-PCR (Fig. 4C, upper). Consistent with this, APN protein about 4 times increased in the iRS cells 24 hours after Dox (2 μg/mL) treatment (Fig. 4B).

To examine whether cell death is induced by human APN overexpression in the human iRS clones, the number of surviving iRS cells was counted after culturing in the presence or absence of 2 μg/mL of Dox. Cells were sub-cultured for 12 hours after the beginning of Dox administration. The number of surviving cells significantly decreased to approximately 35% after culturing for 36 hours in the presence of Dox compared with that in the absence of Dox (Fig. 4C, lower). A visible reduction in the number of iRS cells based on the expression of fluorescent reporter gene, DsRed, occurred 24 and 36 hours after Dox treatment (Fig. 4D).

2.7 | Truncated protein form of nucleus-localized APN

To understand the mechanisms involved in the transport of monomer APN protein from the cytoplasm to the nucleus, human iRS and mouse ES cells were immuno-stained with an antibody recognizing the human N-terminal hyper-variable region of APN (Nt1) (Fig. 5A, upper). The Nt1 antibody is reacted with human APN, but not mouse Apn (Supplementary material Fig. S3). Expectedly, positive Nu Apn signals were detected with the Ct1 antibody, but not with the Nt1 antibody in mouse ES cells without human APN overexpression. Unexpectedly, even in human iRS cells without human APN overexpression, Nu APN signals were undetected with the Nt1 antibody, but detected by the Ct1 antibody (Fig. 5A, lower panels). These data indicated that Nu APN was truncated by missing the Nt1 recognition site. To verify the truncation of Nu APN, western blot hybridization analyses were performed with the Ct1 and Nt1 antibodies. No 30-kDa APN band was detected with the Nt1 antibody in the nuclear fraction of human iRS overexpressing human APN, and mouse ES cells overexpressing human APN (Fig. 5B, left panels). Re-hybridization of the same blot with the Ct1 antibody revealed a 30-kDa band in human iRS cells overexpressing human APN and mouse ES cells overexpressing human APN (Fig. 5B, left panels). Nucleus-localized APN was characterized by truncation with the N-terminal region (Supplementary material Fig. S3). Reactivity of Nt1 to human APN was shown in the product data sheet with human serum APN as a positive

control. Furthermore, intact Cy APN, but not truncated Nu APN, was positively reacted with Nt1 in MEFs overexpressing human APN (Fig. 5B, right panels; Supplementary material Fig. S4). Truncated Nu APN/Apn was, however, detected with Ct1 in the same slide (Fig. 5B, right panels; Supplementary material Fig. S4). Collectively, human and mouse Nu APN/Apn proteins formed truncated APN/Apn proteins missing the hyper-variable region and N-terminal signal peptide.

2.8 | Function of nucleus-localized APN

To predict the molecular function of nuclear APN, genome-wide gene expression changes between Dox (-) and Dox (+) iRS cells were analyzed using a human Affymetrix GeneChip microarray system. A Dox-dependent increase of APN was detected by RT-PCR before the genome-wide gene expression analysis (Fig. 6A). Comparative analysis demonstrated similar gene expression profiles between Dox (-) and Dox (+) iRS cells as indicated by an $R^2 = 0.9696$ (Fig. 6A). For the relative value of Dox (+) to Dox (-), 1043 genes had more than 1.5 times a higher expression level, and 610 genes had less than 1.5 times a lower expression level. Pathway enrichment analysis demonstrated statistically significant differences between Dox (-) and Dox (+) states in post-transcriptional silencing by small RNAs by Reactome, post-translational regulation of the

adherens junction by NCI-Nature, and chromatin remodeling by hSWI/SNF by BioCarta (Fig. 6B). These results indicated that Nu adiponectin played a role in microRNA-mediated post-transcription regulation, cell-cell interactions, and chromatin remodeling.

2.9 | Apoptotic cell death by APN overexpression

In the comparative transcriptome analyses between Dox (-) and Dox (+) iRS cells, expression changes of caspase-independent apoptosis-associated genes, *AIFM2* and *MEG3*, were significant, but no significant change of caspase-dependent apoptosis-related genes, *BAX*, *BCL2*, *CASPASE-3*, and *CASPASE-9*, were revealed (Fig. 6C). To verify these findings, comparative qPCR analyses between Dox (-) and Dox (+) iRS cells were performed. The expression level of *AIFM*2 and *MEG3* significantly increased in Dox (+) iRS cells (Fig. 6D). Furthermore, miR-214-3p, which is a microRNA inversely associated with *MEG3* in a post-transcriptional manner (Fan et al., 2017), significantly decreased in Dox (+) iRS cells as detected by miRNA qPCR analyses (Fig. 6D). No significant change of miR-214-5p between Dox (-) and Dox (+) iRS cells was detected (Supplementary material Fig. S5). To verify direct relationship between APN overexpression and AIFM2-mediated cell death, rescue experiments were performed by the treatment with miR-214-3p

mimic (Fig. 6E). The number of cells was counted at 0 and 24 hours after Dox treatment, and RNA was extract from cells 24 hours after Dox treatment (Fig. 6E, lower). miR-214 mimic transfection induced significant increase of survival rate of APN-overexpressing iRS cells as a consequence of downregulation of *AIFM2* expression. Therefore, the MEG3-miR-214-AIFM2 pathway worked on apoptotic cell death in APN-overexpressed iRS cells (Fig. 6F).

3 | DISCUSSION

Here, we demonstrated that intracellular APN/Apn was differentially localized in a Nu or Cy-type in primary culture from embryos and various somatic tissues and localized to the nucleus in mouse ES cells and human iPS and iRS cells. In human iRS and mouse ES cells, Nu APN/Apn existed as a monomer in contrast with its multimer forms observed in Cy-type adipose cells. The monomer APN/Apn showed a truncated form missing the hyper-variable region and N-terminal peptide. Dox-inducible overexpression of APN induced cell death in human iRS and mouse ES cells. Comparative genome-wide gene expression analysis between Dox (-) and Dox (+) iRS cells revealed caspase-independent apoptosis from APN overexpression. Caspase-independent apoptosis-related genes, *AIFM2* and *MEG3*, were upregulated, and miR-214-3p was downregulated by APN

overexpression. Cell death by APN overexpression was rescued by miR-214-3p mimic transfection to iRS cells. Pathway enrichment analysis demonstrated that the Nu APN/Apn may function in microRNA-mediated post-transcription regulation, cell-cell interactions, and chromatin remodeling.

Aging, which is defined as a chronic decline in tissue function due to the decrease of physical resilience, is inevitable in mammals. A slower progression of aging is desirable for extending human life span. In mouse heterochronic parabiosis experiments, which involves the surgical parabiotic pairing of aged and young mice to exchange blood, factors in blood derived from the young mouse revitalized the organs, including the liver, muscle, and brain, in the old mouse (Rebo et al., 2016). Furthermore, slowing aging of stem cells and their niche may slow tissue and organismal aging (Conboy & Rando, 2012). Aging is, at least in part, explained by the chronic decline of youth factors over time. Plasma Apn, an adipokine circulating throughout the body in the blood, is a candidate youth factor. Plasma Apn has a crucial role in the promotion of insulin sensitization and improves whole-body energy homeostasis (Schraw et al., 2008). The positive effects from the pleiotropic functions of plasma Apn suggest that Apn overexpression slows aging. This is consistent with the longevity of tempospatially specific Apn-overexpressing transgenic mice (Yamauchi et al., 2003b; Combs et al., 2004; Otabe et al., 2007), but is inconsistent with the embryonic lethality and adult sterility in ubiquitously Apn-overexpressing mice (Combs et al., 2004). Nuclear Apn expression was

detected in mouse germ cell precursors, PGCs (Fig. 1B), and in somatic cells surrounding PGCs. Apoptotic cell death induced by overexpression of Apn in germ cells or gonadal somatic cells causes sterility because of the poor development of germ cells in transgenic mice.

An unexpected finding was that a monomeric form of APN/Apn was localized in the nuclei of human iPS/iRS and mouse ES cells regardless of the thermodynamic instability of the Apn monomer isoform (Shapiro & Scherer, 1998; Wang & Scherer, 2008). Post-translational glycosylation at lysine 68, 71, 80, and 104 was reported (Wang, Xu, Knight, Xu, & Cooper, 2002) to be involved in the assembly and secretion of HMW Apn (Wang et al., 2006). Furthermore, cysteine 39 in mouse Apn and cysteine 36 in human APN play a role in multimerization (Pajvani et al., 2003). Human monomeric Nu APN is truncated by the lack of Nt1-recongnition site including cysteine 36 in APN (Fig. 5A: Supplementary material Fig. S3). To generate truncated APN/Apn, tissue-specific protease activity after neo-APN/Apn protein is synthesized in the cytoplasm and before multimerization, is required (Fig. 7). An unidentified enzyme catalyzing the truncation of APN/Apn protein may determine cellular localization and function. Furthermore, the missing N-terminal signal peptide may change the localization of APN/Apn from the cytoplasm to the nucleus. The importin α/β-dependent nuclear transport system is involved in nucleocytoplasmic shuttling. A cargo protein with a nuclear localization signal is recognized by importin α, and a ternary complex with importin β is formed. The

cargo/importin α/β complex can enter the nucleus through interactions with the nuclear pore complex (Yasuhara, Oka, & Yoneda, 2009). Truncated but not intact APN/Apn can be selectively captured by the nuclear transporter in a tissue-specific manner (Yasuhara et al., 2007). It remains unclear which nuclear transporter recruits truncated APN/Apn into the nucleus.

Apoptotic cell death in human iRS and mouse ES cells by overexpression of Nu APN suggests that nuclear APN/Apn controls apoptosis by its accumulation level. Caspase-independent apoptosis through the MEG3-miR-214-AIFM2 pathway is a consequence of the physiological reaction against aberrant cellular states in which considerable accumulation of nuclear APN/Apn occurs. *AIFM2* is a homologue of *AIF* (*apoptosis inducing factor*), which is a caspase-independent oxidoreductase located in the mitochondrial membrane (Susin et al., 1999). Upregulation of AIFM2 induces chromosomal condensation and large-scale fragmentation by translocation from the mitochondria to the nucleus, which causes nuclear apoptosis (Fig. 6F). AIFM2 is downregulated by the binding of miR-214-3p in the 3'-UTR of *AIFM2* (Fan et al., 2017), but the binding site of miR-214-3p to *AIFM2* is elusive. miR-214-3p is downregulated by the direct binding of long non-coding RNA (LncRNA) transcribed from *MEG3* (LncRNA-MEG3) (Fan *et al*., 2017). Therefore, similar to T-cell lymphoblastic lymphoma, the MEG3-miR-214-AIFM2 pathway plays a role in apoptotic cell death induced by overaccumulation of nuclear APN/Apn (Fig. 6F). Multimerization of APN/Apn disabling

nuclear translocation may protect from apoptotic cell death of adipocytes by preventing overaccumulation of APN/Apn in nuclei.

Genome-wide gene expression analysis predicts that endogenous APN/Apn functions in post-transcriptional silencing by small RNAs, post-translational regulation of the adherens junction, and chromatin remodeling by hSWI/SNF (Fig. 6B, Fig. 7). In addition, lysine degradation in the lysine catabolic pathway by KEGG, the Ras signaling pathway by Panther, and XPodNet protein-protein interaction by the WikiPathways were discovered as pathways significantly related to the functions of Nu APN/Apn. MicroRNA-mediated post-transcriptional regulation is repeatedly listed in database analyses as related to APN/Apn functions. Upregulation of *APN/Apn* is associated with the upregulation of *MEG3*, which has a role in carcinogenesis, lipid metabolism, and fibrotic disease by the regulation of several downstream microRNAs. Expression of LncRNA-MEG3 is regulated by miR-29 (Braconi et al., 2011) and miR-148a (Yan et al., 2014) through modulation of DNA methylation. APN/Apn overaccumulation in nuclei may induce hypomethylation of the *MEG3* promoter, but it remains unclear how nuclear APN/Apn directly regulates the expression of *MEG3* (Fig. 6F).

An increase in APN/Apn levels may contribute to longevity through anti-obesity and anti-inflammation effects in humans. Here, we demonstrated a novel function of nuclear APN/Apn as a survival gate keeper different from plasma APN/Apn, which impedes aging. Pharmaceutical and medical applications of APN should increase plasma APN without upregulating nuclear APN to increase human longevity.

4 | EXPERIMENTAL PROCEDURES

4.1 | Primary culture of somatic cells

For MEF generation, 12.5 *dpc* (*days post coitum*) embryos collected from ICR females (Japan SLC, Shizuoka, Japan) were disaggregated using a 2.5-mL syringe with an 18-gauge needle. MEFs were cultured in MEF medium (Yamaguchi, Hirano, Nagata, & Tada, 2011). For primary culture cells from adult mice, organs and tissues collected by dissection of 8-week-old female ICR mice (Japan SLC) were minced with surgical scissors. Cells and cell clumps were cultured in MEF medium.

4.2 | Culture of pluripotent stem cells

Mouse R1 ES cells (Nagy, Rossant, Nagy, Abramow-Newerly, & Roder,1993) were maintained in ES cell medium on MEF feeder cells (Sun et al., 2014). Human iPS and iRS cells were cultured on feeder-free Matrigel-coated dishes with MEF-conditioned iPS cell medium (CM) (Teshigawara et al., 2016). iRS cells were stably maintained in CM through subculture at a density of 1.0 x 10^6 cells per Matrigel-coated 10-cm dish and subcultured by dissociation with conventional trypsin (Gibco; Thermo Fisher Scientific, Waltham, MA). Human iRS cell was established cell line as pre-iPS cell by transduction of exogenous *Oct4, Sox2, Klf4, c-Myc* and *DsRed* genes (Teshigawara et al., 2016). DsRed was a fluorescent marker for visualizing the activity of reprogramming factors, Oct4, Sox2, Klf4, and c-Myc. Exogenous *DsRed* was stably expressed in iRS cells under a maintaining state, in which reprogramming into iPS cells was paused. Exogenous *DsRed* was used as a marker for quantitative standardization of qPCR for microRNA transcription. For rescue experiments of cell death, hsa-miR-214-3p miRNA mimic or mock (100 pmol/mL) (Abm, Vancouver, Canada) was transfected to Dox-inducible APN overexpression iRS cells with Lipofectamine 2000 (Thermo Fisher scientific) according to the manufacturer's protocol, 60 hours before the beginning of Dox treatment. For induction of APN expression, 2 μg/mL Dox was administered in the culture of iRS and ES cells.

4.3 | Preparation of primordial germ cells

For isolation of PGCs, genital ridges of 12.5 *dpc* embryos collected from Oct4-GFP transgenic mice (Kimura et al., 2015) were pipetted in 0.05% trypsin/EDTA. After washing with phosphate buffer (PB1)/3 mg/mL bovine serum albumin (BSA) solution, PGCs re-suspended in DMEM with 10% FBS (Gibco) were sorted by GFP expression using FACS Aria II flow cytometry (BD Bioscience, Franklin Lakes, NJ). After rinsing with phosphate-buffered saline (PBS), purified PGCs dropped on slides were dipped in 1% paraformaldehyde (PFA) fixative in distilled water (DW) (pH 9.2) containing 0.15% Triton X-100 and 3 mM dithiothreitol (Sigma-Aldrich, St. Louis, MO). The slides were incubated overnight at 4 °C, washed in 0.4% Photo-Flo (Kodak, Rochester, NY) in DW, and then dried.

4.4 | RT-PCR

Total RNA (10 μg) extracted from tissues and cultured cells using TRIzol (Invitrogen; Thermo Fisher Scientific) was treated with recombinant DNase I (Takara, Shiga, Japan) and used for cDNA synthesis following the manufacturer's instructions (Teshigawara et al., 2016). Synthesized cDNA was PCR-amplified with Ex-Taq (Takara) using gene-specific primers. For quantitative RT-PCR

(qPCR), THUNDERBIRD SYBR qPCR Mix (Toyobo, Osaka, Japan) was used according to the manufacturer's instructions. For microRNA qPCR, miScript II RT Kit (QIAGEN, Hilden, Germany) was used for reverse transcription with HiFlex buffer. cDNA was qPCR-amplified using miScript SYBR Green PCR Kit (QIAGEN) with the universal reverse and miRNA-specific primers according to the manufacturer's instructions. Relative gene expression levels were calculated after normalization to *GAPDH* (for conventional qPCR) or *DsRed* (for microRNA). Exogenous *DsRed*, which was stably expressed in all iRS cells was used for standardization of the qPCR of microRNA, instead of unstable U6. The primer sequences are summarized in Supplementary material Table S1.

4.5 | Western blot hybridization

Whole cell extracts were prepared with lysis buffer without 2-mercaptoethanol (native) or with 10% 2-mercaptoethanol at 95 °C (reduced) (Kuroda et al., 2005). Nuclear and cytoplasmic proteins were separately extracted with the Nuclear/Cytosolic Fractionation Kit (Cell Biolabs, San Diego, CA) following the manufacturer's instructions. The protein concentration was measured using the DC™ protein assay kit (Bio-Rad, Hercules, CA). Freshly prepared lysates were separated on 10% SDS-polyacrylamide gels, and then blotted onto Immobilon polyvinylidene difluoride (PVDF)

membranes (Millipore, Billerica, MA). Membranes were pre-hybridized with blocking solution and then probed with anti-Apn C-terminal-specific antibody 1 (Ct1) (Sigma-Aldrich, Cat# A6354) diluted at 1:1000 or anti-Apn N-terminal-specific antibody 1 (Nt1) (MBL International, Cat# CY-P1031) diluted at 1:500 in 5% BSA in phosphate-buffered saline/0.1% Triton X-100 (PBST) overnight at 4 °C. Membranes were incubated with a horseradish peroxidase (HRP)-linked anti-rabbit IgG secondary antibody (GE Healthcare, Chicago, IL, Cat# NA934) diluted at 1:1000 in 5% BSA in PBST for 1 hour at room temperature. Non-specifically bound antibody was removed by washing with PBST six times for 10 minutes each. Bands were visualized by ImageQuant LAS 4010 using the ECL Prime Western Blotting Detection Reagents (GE Healthcare) according to the manufacturer's instructions.

4.6 | Construction of lentiviral vectors and infection

The plasmid TetO-FUW-APN was constructed by modifying the TetO-FUW-OSKM (Oct4, Sox2, Klf4, c-Myc) (Carey et al., 2009) and replacing the OSKM sequence with the full coding sequence (CDS) of human *APN* using a ligation kit (Toyobo, Osaka, Japan) according to the manufacturer's protocol. The full *APN* CDS was constructed from total RNA human adipose tissue (Biochain, Newark, CA). With 10 μg of the packaging construct (pCAG-HIVgp) and 10 μg of VSV-G, the Rev

construct (pCMV-VSV-G-RSV-Rev) and 17 μg of self-inactivating (SIN) lentiviral particles (TetO-FUW-APN or FUW-M2rtTA (Hockemeyer et al., 2008) were packaged into HEK 293T cells. MEF cells (1 x 10^5) were co-infected with collected viral supernatant as described previously (Yamaguchi et al., 2009). The primer sequences are summarized in Supplementary material Table S1.

4.7 | Construction and transfection of APN overexpression vector

The full CDS of human *APN* was inserted into the NheI-BamHI site of a Dox-inducible vector pCW57.1 (Addgene plasmid #41393). The Dox-inducible pCW57.1-APN vector (50 μg) was electroporated into 1.0 x 10^7 of human iRS and mouse ES cells in a cuvette with a 4-mm electrode gap (Flowgen, Nottingham, UK) using Gene Pulser (Bio-Rad) at 250 V and 500 μF. Then, 5.0 x 10^6 cells were transferred onto MEF feeders in 10-cm dishes with ES medium for mouse ES cells, and feeder-free Matrigel-coated 10-cm dishes with MEF-conditioned iPS medium for human iRS cells. Cells were drug-selected with puromycin (2.0 μg/mL for mouse ES cells and 0.5 μg/mL for human iRS cells) (Invitrogen). The selection medium was changed every 24 hours. After cell expansion, clones were isolated using sterilized glass pipettes.

4.8 | Immunocytochemistry

Cultured cells were fixed with 4% PFA/PBS for 10 minutes at room temperature and then pre-treated with blocking solution (3% BSA, 2% skim milk (BD Bioscience) in PBST) for 1 hour at room temperature. PGCs were pre-treated with blocking solution (3% BSA in 0.1% Tween-20) for 1 hour at room temperature after permeabilization with 0.5% Triton X-100 for 15 minutes. Cells were immuno-reacted with anti-Apn antibody Ct1 (diluted at 1:500), Nt1 (diluted at 1:250), or anti-Apn C-terminal-specific antibody 2 (Ct2) (diluted at 1:500) (Novus, Cat# NB100-65810) overnight at 4 °C, and then incubated with the secondary Alexa 488 (green) (Cat# A-11008) or Alexa 546 (red) (Cat# A-11010) anti-rabbit antibody (Thermo Fisher Scientific) diluted at 1:200 in blocking buffer for 1 hour. Samples were stained with DAPI and mounted with Slowfade Gold Antifade Reagent (Invitrogen).

4.9 | Alkaline phosphatase staining

Mouse ES cells were fixed with 4% PFA for 10 minutes at room temperature. Alkaline phosphatase enzyme activity in mouse ES cells was detected by treatment with 2:1:1 mixture of Fast

Red TR (0.8 mg/mL)-Naphthol AS-MX phosphatase solution (4 mg/mL)-DW (Sigma-Aldrich) in the dark for 15 minutes following the manufacturer's instructions.

4.10 | Microarray

Labeled total RNA (1 μg) was hybridized with the Human Genome U133 plus 2.0 Array (Affymetrix; Thermo Fisher Scientific) according to the manufacturer's instructions. Heat map and scatter plot analyses were performed as described previously (Teshigawara et al., 2016). For pathway enrichment analysis, differentially expressed genes between Dox (-) and Dox (+) iRS cells ($p < 0.05$, fold change > 1.5) were selected and mapped to databases with Enrichr software. The top three enriched pathways were ranked by an Enrichr combined score ($p < 0.05$) as the relative value. The combined score 'c' is defined as $c = \log(p) \times z$, where p refers to the *p*-value from the Fisher's exact test, and z is the z-score indicating the deviation from the expected rank.

4.11 | Statistical analysis

Bar graphs were presented as the mean ± s.e.m. from at least three independent experiments. Two-tailed Student's t-tests were performed using Microsoft Excel software. The *p*-values were considered significant at $*p < 0.05$, $**p < 0.01$ and $***p < 0.001$.

ACKNOWLEDGEMENTS

We thank Ms. Megumi Fukuchi for preparing the experiments and Ms. Ayane Masumoto for collecting the PGCs. J.C. is a fellow of the Japanese government (Ministry of Education, Culture, Sports, Science and Technology; MEXT), and R.T. is a fellow of the Grant-in-Aid for Japan Society for Promotion of Science (JSPS).

AUTHORS' CONTRIBUTIONS

Conceptualization: T.T.; Methodology: J.C., R.T., M.K., S.Y., T.T.; Investigation: J.C., R.T., M.K.; Writing: J.C., R.T., T.T.; Supervision: T.T.

ORCID

Takashi Tada ID; http://orcid.org/0000-0003-1172-2685

REFERENCES

Achari, A. E., & Jain, S. K. (2017). Adiponectin, a therapeutic target for obesity, diabetes, and endothelial dysfunction. *Int. J. Mol. Sci. 18*, 1321. https://doi.org/10.3390/ijms18061321.

Bauche, I. B., Ait, E. l., Mkadem, S., Rezsohaz, R., Funahashi, T., Maeda, N., … Brichard, S. M. (2006). Adiponectin downregulates its own production and the expression of its AdipoR2 receptor in transgenic mice. *Biochem. Biophys. Res. Commun. 345*, 1414–1424. https://doi.org/10.1016/j.bbrc.2006.05.033.

Bauche, I. B., El Mkadem, S. A., Pottier, A. M., Senou, M., Many, M. C., Rezsohazy, R., … Brichard, S. M. (2007). Overexpression of adiponectin targeted to adipose tissue in transgenic mice: Impaired adipocyte differentiation. *Endocrinology 148*, 1539–1549. https://doi.org/10.1210/en.2006-0838.

Braconi, C., Kogure, T., Valeri, N., Huang, N., Nuovo, G., Costinean, S., … Patel. T. (2011). microRNA-29 can regulate expression of the long non-coding RNA gene MEG3 in hepatocellular cancer. *Oncogene. 30*, 4750-4756. https://doi.org/10.1038/onc.2011.193.

Carey, B. W., Markoulaki, S., Hanna, J., Saha, K., Gao, Q., Mitalipova, M., & Jaenisch, R. (2009) Reprogramming of murine and human somatic cells using a single polycistronic vector. *Proc. Natl. Acad. Sci. 106*, 157–162. https://doi.org/10.1073/pnas.0811426106.

Combs, T. P., Pajvani, U. B., Berg, A. H., Lin, Y., Jelicks, L. A., Laplante, M., … Scherer, P.E. (2004). A transgenic mouse with a deletion in the collagenous domain of adiponectin displays elevated circulating adiponectin and improved insulin sensitivity. *Endocrinology 145*, 367–383. https://doi.org/10.1210/en.2003-1068.

Conboy, I. M., & Rando, T.A. (2012). Heterochronic parabiosis for the study of the effects of aging on stem cells and their niches. *Cell Cycle 11*, 2260–2267. https://doi.org/10.4161/cc.20437.

Fan, F. Y., Deng, R., Yi, H., Sun, H. P., Zeng, Y., He, G.C., & Su, Y. (2017). The inhibitory effect of MEG3/miR-214/AIFM2 axis on the growth of T-cell lymphoblastic lymphoma. *Int. J. Oncol. 51*, 316-326. https://doi.org/10.3892/ijo.2017.4006.

Hockemeyer, D., Soldner, F., Cook, E. G., Gao, Q., Mitalipova, M., & Jaenisch, R. (2008). A drug-inducible system for direct reprogramming of human somatic cells to pluripotency. *Cell Stem Cell 3*, 346–353. https://doi.org/10.1016/j.stem.2008.08.014.

Hug. C., Wang. J., Ahmad, N. S., Bogan, J. S., Tsao, T-S., & Lodish, H.F. (2004). T-cadherin is a receptor for hexameric and high-molecular-weight forms of Acrp30/adiponectin. *Proc. Natl. Acad. Sci. 101*, 10308–10313. https://doi.org/10.1073/pnas.0403382101.

Jin, X., Chen, J., Hu, Z., Chan, L., & Wang, Y. (2013). Genetic deficiency of adiponectin protects against acute kidney injury. *Kidney Int. 83*, 604–614. https://doi.org/10.1038/ki.2012.408.

Kimura, T., Kaga, Y., Sekita, Y., Fujikawa, K., Nakatani, T., Odamoto, M., … Nakano, T. (2015). Pluripotent stem cells derived from mouse primordial germ cells by small molecule compounds. *Stem Cells 33*, 45–55. https://doi.org/10.1002/stem.1838.

Kubota, N., Terauchi, Y., Yamauchi, T., Kubota, T., Moroi, M., Matsui, J., … Noda, T. (2002). Disruption of adiponectin causes insulin resistance and neointimal formation. *J. Biol. Chem. 277*, 25863–25866. https://doi.org/10.1074/jbc.C200251200.

Kuroda, T., Tada, M., Kubota, H., Kimura, H., Hatano, S., Suemori, H., … Tada, T. (2005). Octamer and Sox elements are required for transcriptional cis regulation of Nanog gene expression. *Mol. Cell. Biol. 25*, 2475-2485. https://doi.org/10.1128/MCB.25.6.2475-2485.2005.

Liao, Y., Takashima, S., Maeda, N., Ouchi, N., Komamura, K., Shimomura, I., … Kitakaze, M. (2005). Exacerbation of heart failure in adiponectin-deficient mice due to impaired regulation of AMPK and glucose metabolism. *Cardiovasc. Res. 67*, 705–713. https://doi.org/10.1016/j.cardiores.2005.04.018.

Maeda, N., Shimomura, I., Kishida, K., Nishizawa, H., Matsuda, M., Nagaretani, H., … Matsuzawa, Y. (2002). Diet-induced insulin resistance in mice lacking adiponectin/ACRP30. *Nat. Med. 8*, 731–737. https://doi.org/10.1038/nm724.

Matsumoto, H., Tamura, S., Kamada, Y., Kiso, S., Fukushima, J., Wada, A., … Hayashi, N. (2006). Adiponectin deficiency exacerbates lipopolysaccharide/D-galactosamine-induced liver injury in mice. *World J. Gastroenterol. 12*, 3352–3358. https://doi.org/10.3748/wjg.v12.i21.3352.

Nagy, A., Rossant. J., Nagy, R., Abramow-Newerly, W., & Roder, J.C. (1993). Derivation of completely cell culture-derived mice from early-passage embryonic stem cells. *Proc. Natl. Acad. Sci. 90*, 8424-8428. https://doi.org/10.1073/pnas.90.18.8424.

Nawrocki, A. R., Rajala, M. W., Tomas, E., Pajvani, U. B., Saha, A. K., Trumbauer, M. E., … Scherer, P. E. (2006), Mice lacking adiponectin show decreased hepatic insulin sensitivity and reduced responsiveness to peroxisome proliferator-activated receptor γ agonists. *J. Biol. Chem. 281*, 2654–2660. https://doi.org/10.1074/jbc.M505311200.

Otabe, S., Yuan, X., Fukutani, T., Wada, N., Hashinaga, T., Nakayama, H., … Yamada, K. (2007). Overexpression of human adiponectin in transgenic mice results in suppression of fat accumulation and prevention of premature death by high-calorie diet. *Am. J. Physiol. Endocrinol. Metab. 293*, E210–E218. https://doi.org/10.1152/ajpendo.00645.2006.

Ouchi, N., Ohishi, M., Kihara, S., Funahashi, T., Nakamura, T., Nagaretani, H., … Matsuzawa, Y. (2003). Association of hypoadiponectinemia with impaired vasoreactivity. *Hypertension 42*, 231–234. https://doi.org/10.1161/01.HYP.0000083488.67550.B8.

Pajvani, U. B., Du, X., Combs, T. P., Berg, A. H., Rajala, M. W., Schulthess, T., Engel, J., … Scherer, P. E. (2003). Structure-function studies of the adipocyte-secreted hormone Acrp30/adiponectin: Implications for metabolic regulation and bioactivity. *J. Biol. Chem. 278*, 9073–9085. https://doi.org/10.1074/jbc.M207198200.

Rebo, J., Mehdipour, M., Gathwala, R., Causey, K., Liu, Y., Conboy, M. J., & Conboy, I. M. (2016). A single heterochronic blood exchange reveals rapid inhibition of multiple tissues by old blood. *Nat. Commun. 7*, 13363. https://doi.org/10.1038/ncomms13363.

Scherer, P. E., Williams, S., Fogliano, M., Baldini, G., & Lodish, H. F. (1995). A novel serum protein similar to C1q, produced exclusively in adipocytes. *J. Biol. Chem. 270*, 26746–26749. https://doi.org/10.1074/jbc.270.45.26746.

Schraw, T., Wang, Z. V., Halberg, N., Hawkins, M., & Scherer, P. E. (2008). Plasma adiponectin complexes have distinct biochemical characteristics. *Endocrinology 149,* 2270–2282. https://doi.org/10.1210/en.2007-1561.

Shapiro, L., & Scherer, P. E. (1998). The crystal structure of a complement-1q family protein suggests an evolutionary link to tumor necrosis factor. *Curr. Biol. 8*, 335–338. https://doi.org/10.1016/S0960-9822(98)70133-2.

Sun, L. T., Yamaguchi, S., Hirano, K., Ichisaka, T., Kuroda, T., & Tada, T. (2014). Nanog co-regulated by Nodal/Smad2 and Oct4 is required for pluripotency in developing mouse epiblast. *Dev. Biol. 392*, 182-192. https://doi.org/10.1016/j.ydbio.2014.06.002.

Sun, Y., Xun, K., Wang, C., Zhao, H., Bi, H., Chen, X., & Wang, Y. (2009). Adiponectin, an unlocking adipocytokine. *Cardiovasc. Ther. 27*, 59–75. https://doi.org/10.1111/j.1755-5922.2008.00069.x.

Susin, S. A., Lorenzo, H. K., Zamzami, N., Marzo, I., Snow, B. E., Brothers, G. M., … Kroemer, G. (1999). Molecular characterization of mitochondrial apoptosis-inducing factor. *Nature.* 397, 441-446. https://doi.org/10.1038/17135.

Teshigawara, R., Hirano, K., Nagata, S., Ainscough, J., & Tada, T. (2016). OCT4 activity during conversion of human intermediately reprogrammed stem cells to iPSCs through mesenchymal-epithelial transition. *Development. 143*, 15-23. https://doi.org/10.1242/dev.130344.

Wang, Y., Lam, K. S. L, Chan, L., Kok, W. C., Lam, J. B. B., Lam, M. C., … Xu, A. (2006). Post-translational modifications of the four conserved lysine residues within the collagenous domain of adiponectin are required for the formation of its high molecular weight oligomeric complex. *J. Biol. Chem. 281*,16391–16400. https://doi.org/10.1074/jbc.M513907200.

Wang, Z. V., & Scherer, P. E. (2008). DsbA-L is a versatile player in adiponectin secretion. *Proc. Natl. Acad. Sci. 105*, 18077–18078. https://doi.org/10.1073/pnas.0810027105.

Wang, Y., Xu, A., Knight, C., Xu, L. Y., & Cooper, G. J. S. (2002) .Hydroxylation and glycosylation of the four conserved lysine residues in the collagenous domain of adiponectin: potential role in the

modulation of its insulin-sensitizing activity. *J. Biol. Chem. 277*, 19521–19529. https://doi.org/10.1074/jbc.M200601200.

Yamaguchi, S., Hirano, K., Nagata, S., & Tada, T. (2011). Sox2 expression effects on direct reprogramming efficiency as determined by alternative somatic cell fate. *Stem Cell Res. 6*, 177-186. https://doi.org/10.1016/j.scr.2010.09.004.

Yamaguchi, S., Kurimoto, K., Yabuta, Y., Sasaki, H., Nakatsuji, N., Saitou, M., & Tada, T. (2009). Conditional knockdown of Nanog induces apoptotic cell death in mouse migrating primordial germ cells. *Development 136*, 4011–4020. https://doi.org/10.1242/dev.041160.

Yamauchi, T., Kamon, J., Ito, Y., Tsuchida, A., Yokomizo, T., Kita, S., … Kadowaki, T. (2003a). Cloning of adiponectin receptors that mediate antidiabetic metabolic effects. *Nature 423*, 762–769. https://doi.org/10.1038/nature01705.

Yamauchi, T., Kamon, J., Waki, H., Imai, Y., Shimozawa, N., Hioki, K., … Kadowaki, T. (2003b). Globular adiponectin protected ob/ob mice from diabetes and ApoE-deficient mice from atherosclerosis. *J. Biol. Chem. 278*, 2461–2468. https://doi.org/10.1074/jbc.M209033200.

Yan, J., Guo, X., Xia, J., Shan, T., Gu, C., Liang, Z., … Jin, S. (2014). MiR-148a regulates MEG3 in gastric cancer by targeting DNA methyltransferase 1. *Med. Oncol. 31*, 879. https://doi.org/10.1007/s12032-014-0879-6.

Yasuhara, N., Oka, M., & Yoneda, Y. (2009). The role of the nuclear transport system in cell differentiation. *Semin. Cell Dev. Biol. 20*, 590–599. https://doi.org/10.1016/j.semcdb.2009.05.003.

Yasuhara, N., Shibazaki, N., Tanaka, S., Nagai, M., Kamikawa, Y., Oe, S., … Yoneda, Y. (2007). Triggering neural differentiation of ES cells by subtype switching of importin-α. *Nat. Cell Biol. 9*, 72–79. https://doi.org/10.1038/ncb1521.

FIGURE LEGENDS

FIGURE 1 Adiponectin expression in cells from mouse tissues. (A) Expression of endogenous Apn protein detected by immunocytochemistry with the Ct1 antibody in tissue-derived primary cells. Recognition sites in the globular domain by C-terminal-specific antibodies, Ct1 and Ct2 (upper panel). Phase; phase contrast (cell morphology), Apn (green) for immuno-reactive cells, DAPI (blue) for nuclei. (B) Expression of endogenous Apn protein by immunocytochemistry with the Ct1 antibody in the primordial germ cells (PGCs) (GFP positive) from 12.5 *days post coitum* Oct4-GFP transgenic mouse embryos. Apn (red) indicating immunoreactive nuclei of PGCs, and DAPI (blue) indicating nuclei of PGCs. Apn; mouse adiponectin. Scale bars: 50 μm in (A) and 100 μm in (B).

FIGURE 2 Selective loss of nucleus-localized mouse primary embryonic fibroblasts by ADIPONECTIN overexpression. (A) Differential localization of endogenous Apn protein in mouse primary embryonic fibroblasts (MEFs) by immunocytochemistry with the Ct1 antibody. Apn (green) nucleus-localized (Nu) and cytoplasm-localized (Cy)-type cells coexist in the heterogeneous MEF population. The Nu-type (blue rectangle) and Cy-type (pink rectangle) cells are enlarged in the second and third row, respectively. DAPI (blue) for nuclei. (B) Cell death by Doxycycline (Dox)-inducible

overexpression of human APN in MEFs. For human APN overexpression, a conventional double plasmid system was introduced by lentiviral transduction into MEFs (upper panel). Representative localization and signal intensity of APN/Apn in Nu- and Cy-type MEFs with or without Dox (left of lower panel) by immunocytochemistry with the Ct1 antibody. Selective loss of the Nu-type MEFs 48 hours after administration of 1 μg/mL Dox (+) (right of lower panel). Percentages of the Nu-type cells to Cy-type cells (100%) were compared between cultures in Dox (-) and Dox (+). The number of APN/Apn-positive cells were counted from four independent experiments. *n*; the total number of cells counted. ***$p < 0.001$. APN; human ADIPONECTIN. Apn; mouse Adiponectin. Scale bars: 100 μm (MEFs) and 25 μm (Nu- and Cy-type) in (A), and 10 μm in (B).

FIGURE 3 Cell death induced by ADIPONECTIN overexpression in mouse embryonic stem cells. (A) Expression and localization of endogenous *Apn* in mouse embryonic stem (ES) cells. Expression of endogenous *Apn* in mouse ES cells by RT-PCR (left panel). APN; human ADIPONECTIN, Apn; mouse Adiponectin. PC; *GAPDH* as a positive control. Nuclear localization of endogenous Apn in mouse ES cells by immunocytochemistry with the Ct1 antibody (right panel). Apn (green) for immunoreactive cells, DAPI (blue) for nuclei. (B) Monomeric APN/Apn protein in mouse ES cells by western blot hybridization analyses (upper panel). Expression of exogenous

monomer APN was increased about 4-fold in Dox (+) compared to Dox (-) 24 hours after 2 μg/mL Dox administration. M; Monomer, T; Trimer, H; Hexamer. Dox; Doxycycline. Western blot hybridization analysis with nuclear/cytoplasmic fractionated proteins collected from Dox (+) ES cells overexpressing human APN (lower panel). Monomer APN was detected in the nuclear but not cytoplasmic protein fraction of Dox (+) ES cells. W; whole cell protein, Cy; cytoplasmic protein, Nu; nuclear protein. (C) Induction of cell death by human APN overexpression in mouse ES cells. The single plasmid system incorporated into mouse ES cells for Dox-inducible overexpression of human *APN* (upper panel). *APN*; the *APN* full coding sequence, *Puro*^{r}; puromycin-resistance gene. Dox dose-dependent expression of *APN* in ES cells (middle panel). PC; *GAPDH* as a positive control. A significant decrease in the number of ES cells by Dox-inducible APN overexpression (lower panel). The number of APN/Apn-positive cells from three independent experiments (at least 100 cells per experiment) was reported as mean ± s.e.m. *n*; the total number of cells counted. $^{**}p < 0.01$, $^{***}p < 0.001$. (D) Visualization of survival ES cells visualized by alkaline phosphatase staining every 12 hours in the presence or absence of Dox treatment. Scale bars: 10 μm in (A), and 100 μm in (D).

FIGURE 4 Cell death induced by ADIPONECTIN overexpression in human intermediately reprogrammed stem cells. (A) Expression and localization of endogenous APN in human pluripotent stem cells. Nuclear localization of endogenous APN in induced pluripotent stem (iPS) and intermediately reprogrammed stem (iRS) cells by immunocytochemistry with the Ct1 antibody (upper panel). APN (green) for immunoreactive cells, DAPI (blue) for nuclei. Expression of endogenous *APN* in iPS and iRS cells by RT-PCR (lower panel). PC; *GAPDH* as a positive control. (B) Monomeric APN protein in human iRS cells by western blot hybridization analyses (upper panel). Expression of monomer APN is increased about 4-fold in Dox (+) compared to Dox (-) 24 hours after 2 μg/mL Dox administration. M; Monomer, Dox; Doxycycline. Western blot hybridization analysis with nuclear/cytoplasmic fractionated proteins collected from Dox (+) iRS cells (lower panel). Monomer APN was detected in the nuclear but not cytoplasmic protein fraction in iRS cells overexpressing human APN. W; whole cell protein, Cy; cytoplasmic protein, Nu; nuclear protein. (C) Induction of cell death by human APN overexpression in human iRS cells. Dox dose-dependent expression of human *APN* in iRS cells (upper panel). PC; *GAPDH* as a positive control. A significant decrease in the number of human iRS cells by Dox-inducible human APN overexpression (lower panel). The number of APN-positive cells from three independent experiments (at least 40 cells per experiment) was reported as mean ± s.e.m. *n*; the total number of cells counted. $*p < 0.05$. (D)

Visualization of survival human iRS cells by human APN overexpression every 12 hours after the presence or absence of Dox treatment. Human iRS cells were marked with the fluorescent reporter protein, DsRed. Scale bars: 10 μm in (A) and 100 μm in (D).

FIGURE 5 Truncation of nucleus-localized adiponectin protein in human and mouse pluripotent stem cells. (A) Nuclear APN with the truncation of N-terminal region. Recognition sites in the variable region by the human N-terminal-specific antibody Nt1 (Supplementary material Fig. S3), and the globular domain by the human and mouse C-terminal-specific antibodies Ct1 and Ct2 (upper panel). Cys36; multimerization site. Reaction of endogenous nuclear APN to N and C-terminal-specific antibodies in human intermediately reprogrammed stem (iRS) and mouse embryonic stem (ES) cells by immunocytochemistry (lower panel). No reaction with human-specific Nt1, and positive reaction with human/mouse-specific Ct1, in mouse ES cells was detected. Unexpectedly, negative reaction with Nt1, while positive reaction with Ct1 was revealed in human iRS cells. Phase; phase contrast (cell morphology). APN (green) for immunoreactive cells. DAPI (blue) for nuclei. (B) Immuno-reaction of nuclear APN to N and C-terminal-specific antibodies (human-specific Nt1 and human/mouse-specific Ct1, respectively) in human iRS and mouse ES cells overexpressing human APN. No band was detected by western blot hybridization with the N-terminal

antibody (Nt1). With the same blot after signal-stripped, the C-terminal antibody (Ct1) revealed a band specific to monomer APN (left panels). Nuclear APN protein was obtained 24 hours after 2 μg/mL Dox administration. Nt1 antibody was immunocytochemically reacted with human intact APN (as a positive control), which was localized in the cytoplasm (Cy) (green), but not reacted with human truncated APN, which was localized in the nucleus (Nu) of MEFs overexpressing human APN. Ct1 antibody was reacted both with Nu and Cy-localized APN/Apn (red) (right panels; Supplementary material Fig. S4). Scale bars: 50 μm in (A), 50 μm in DAPI of (B), and 10 μm in Nt1 and Ct1 of (B).

FIGURE 6 Cell death by induced overaccumulation of nuclear ADIPONECTIN. (A) Scatter plot of gene expression in human intermediately reprogrammed stem (iRS) cells with Dox (-) and Dox (+) states. Red lines indicate a 1.5-fold change in signal intensity. Dox-dependent upregulation of exogenous *APN* in RNA samples used for microarray assays were verified by RT-PCR. PC; *GAPDH* as a positive control. (B) Pathway enrichment analysis. The top three significantly enriched pathways were summarized in each category. (C) Comparative heat map of apoptosis-related genes between Dox (-) and Dox (+). Ind; independent, dep; dependent. (D) Expression change of caspase-independent apoptosis-related genes between Dox (-) and Dox (+) by qPCR. *$p < 0.05$, **$p < 0.01$. (E) Rescue of cell death by the treatment with miR-214-3p mimic in Dox (+) human iRS cells

overexpressing human APN. Expression of *AIFM2* was down-regulated by miR-214-3p mimic in Dox (+) iRS cells (left). The number of survived Dox (+) iRS cells increased by miR-214-3p, but not mock, treatment (right). Experimental time course is exhibited under the histograms. *n*; the total number of cells counted. **p* < 0.05, ***p* < 0.01, NS; no significance. (F) A putative pathway for apoptotic cell death by human APN overexpression. Nuc; nucleus, Cyt; cytoplasm.

FIGURE 7 A schematic model of the molecular form and function of nucleus-localized ADIPONECTIN.

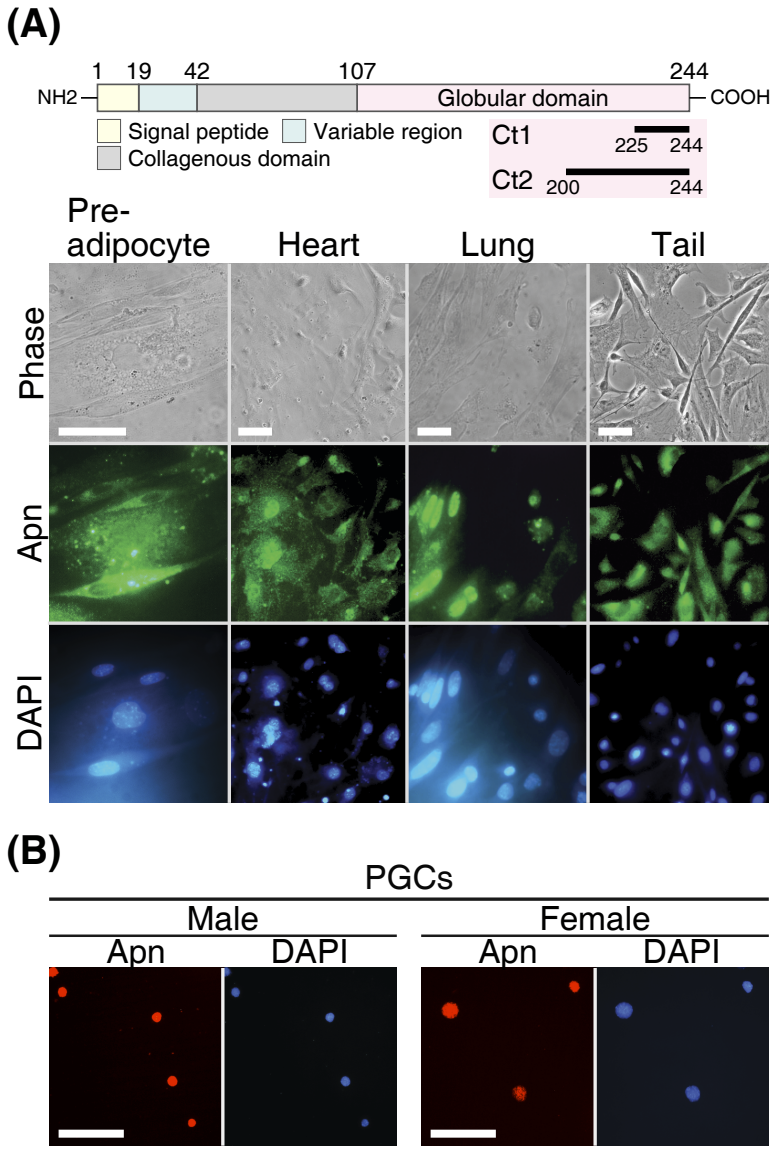
(A)
1
19
42
107
244
NH2
Globular domain
COOH
Signal peptide
Variable region
Collagenous domain
Ct1
225
244
Ct2
200
244
Pre-adipocyte
Heart
Lung
Tail
Phase
Apn
DAPI
(B)
PGCs
Male
Female
Apn
DAPI
Apn
DAPI

Figure 1

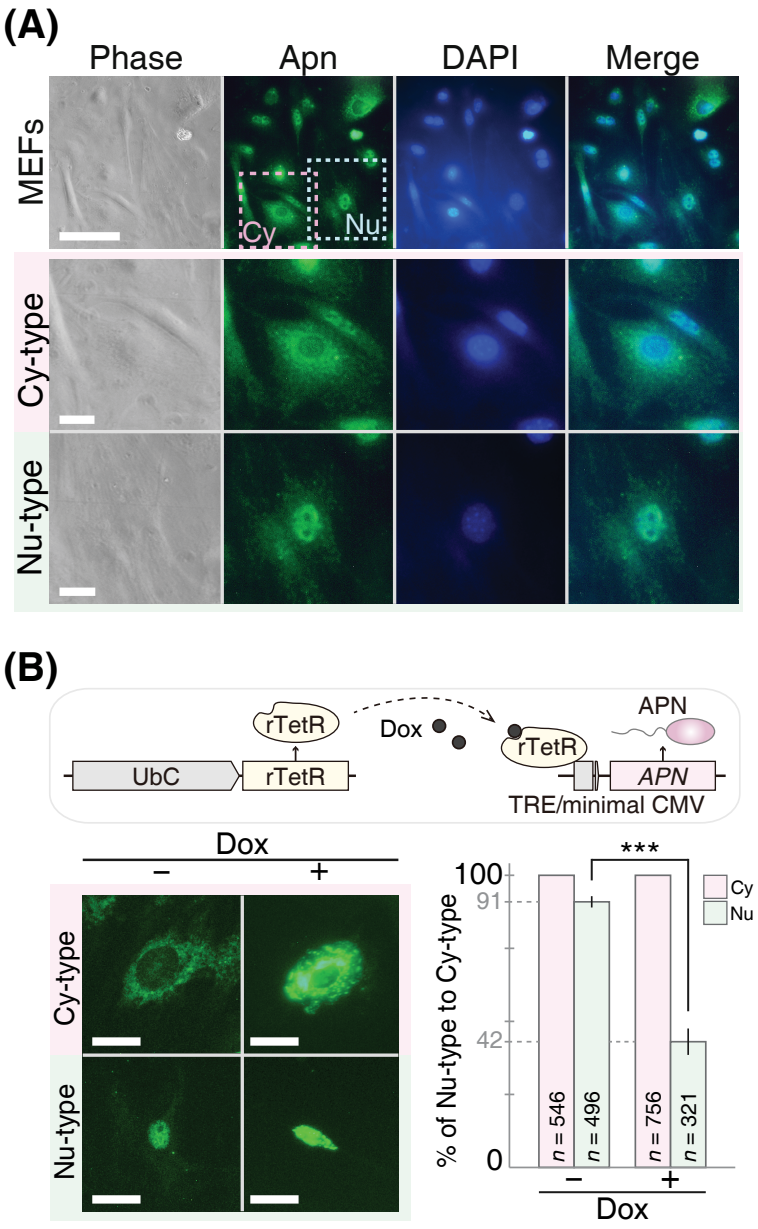
(A)
Phase
Apn
DAPI
Merge
MEFs
Cy
Nu
Cy-type
Nu-type
(B)
rTetR
Dox
APN
rTetR
UbC
rTetR
APN
TRE/minimal CMV
Dox
–
+
Cy-type
Nu-type
***
100
91
42
0
% of Nu-type to Cy-type
Cy
Nu
n = 546
n = 496
n = 756
n = 321
–
+
Dox

Figure 2

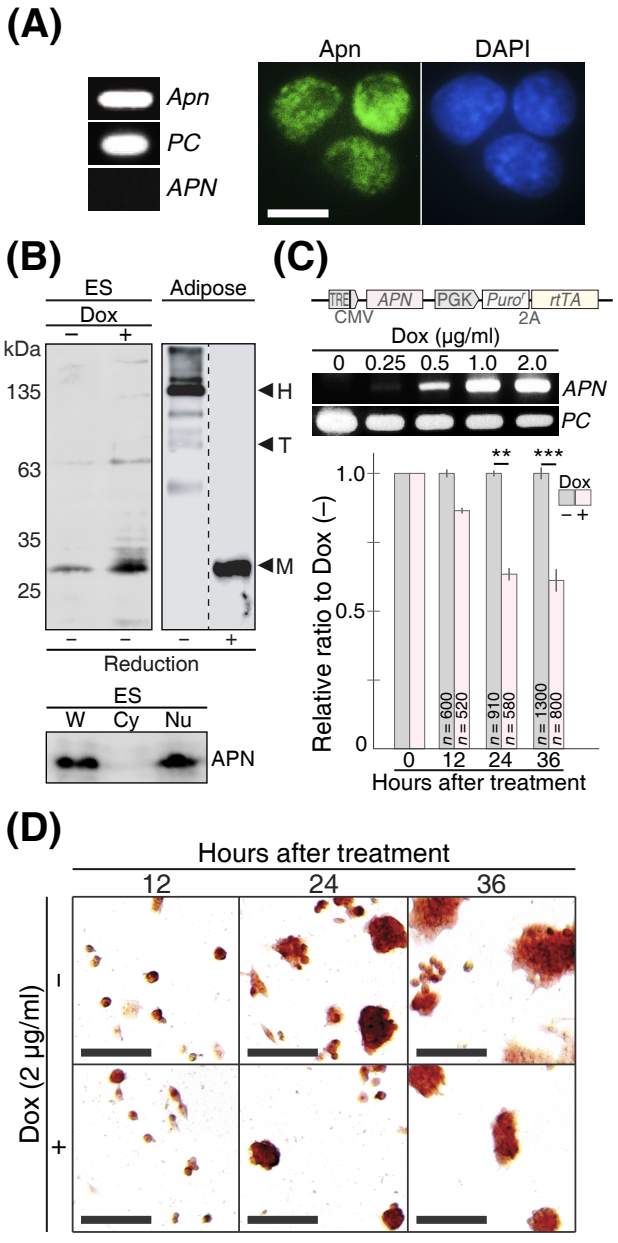
(A)
Apn
DAPI
Apn
PC
APN
(B)
ES
Adipose
Dox
kDa
135
63
35
25
H
T
M
Reduction
ES
W
Cy
Nu
APN
(C)
TRE
CMV
APN
PGK
Puro^r
2A
rtTA
Dox (μg/ml)
0
0.25
0.5
1.0
2.0
APN
PC
Relative ratio to Dox (–)
1.0
0.5
0
**
***
Dox
n = 600
n = 520
n = 910
n = 580
n = 1300
n = 800
0
12
24
36
Hours after treatment
(D)
Hours after treatment
12
24
36
Dox (2 μg/ml)
–
+

Figure 3

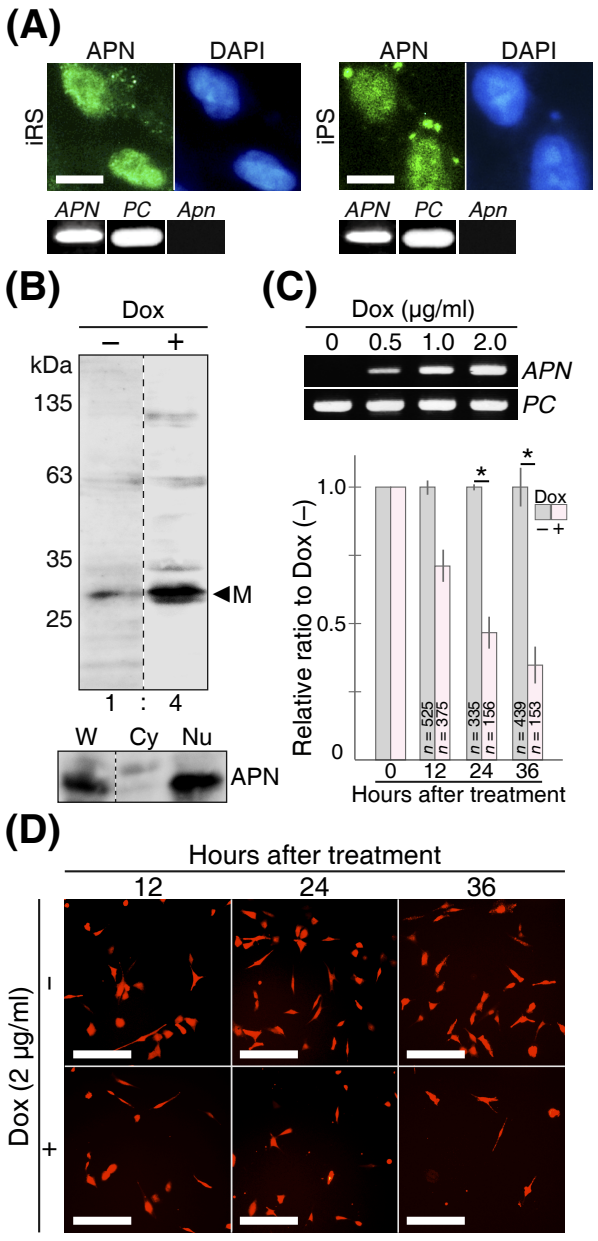
(A)
APN
DAPI
iRS
iPS
APN PC Apn
(B)
Dox
– +
kDa
135
63
35
25
◀M
1 : 4
W Cy Nu
APN
(C)
Dox (μg/ml)
0 0.5 1.0 2.0
APN
PC
Relative ratio to Dox (–)
1.0
0.5
0
Dox
– +
n = 525
n = 375
n = 335
n = 156
n = 439
n = 153
0 12 24 36
Hours after treatment
(D)
Hours after treatment
12 24 36
Dox (2 μg/ml)
–
+

Figure 4

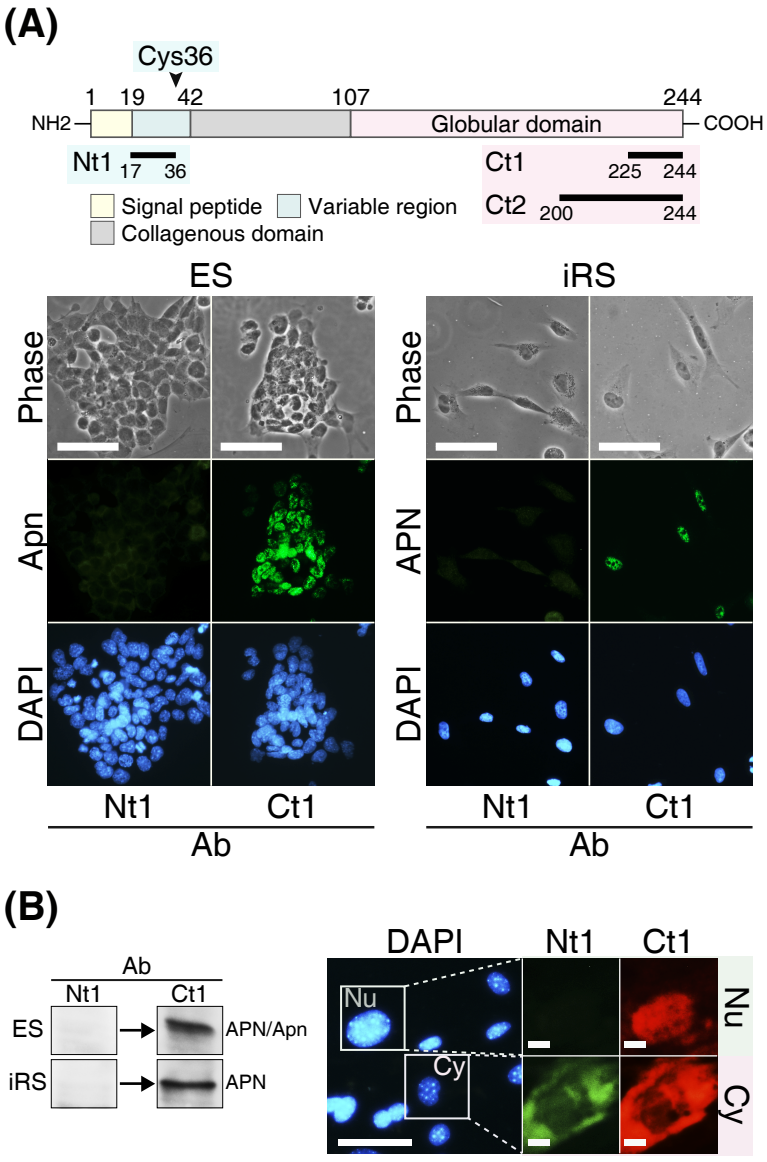
(A)
Cys36
1
19
42
107
244
NH2
Globular domain
COOH
Nt1
17
36
Ct1
225
244
Ct2
200
244
Signal peptide
Variable region
Collagenous domain
ES
iRS
Phase
Apn
APN
DAPI
Nt1
Ct1
Ab
(B)
Ab
Nt1
Ct1
ES
iRS
APN/Apn
APN
DAPI
Nt1
Ct1
Nu
Cy

Figure 5

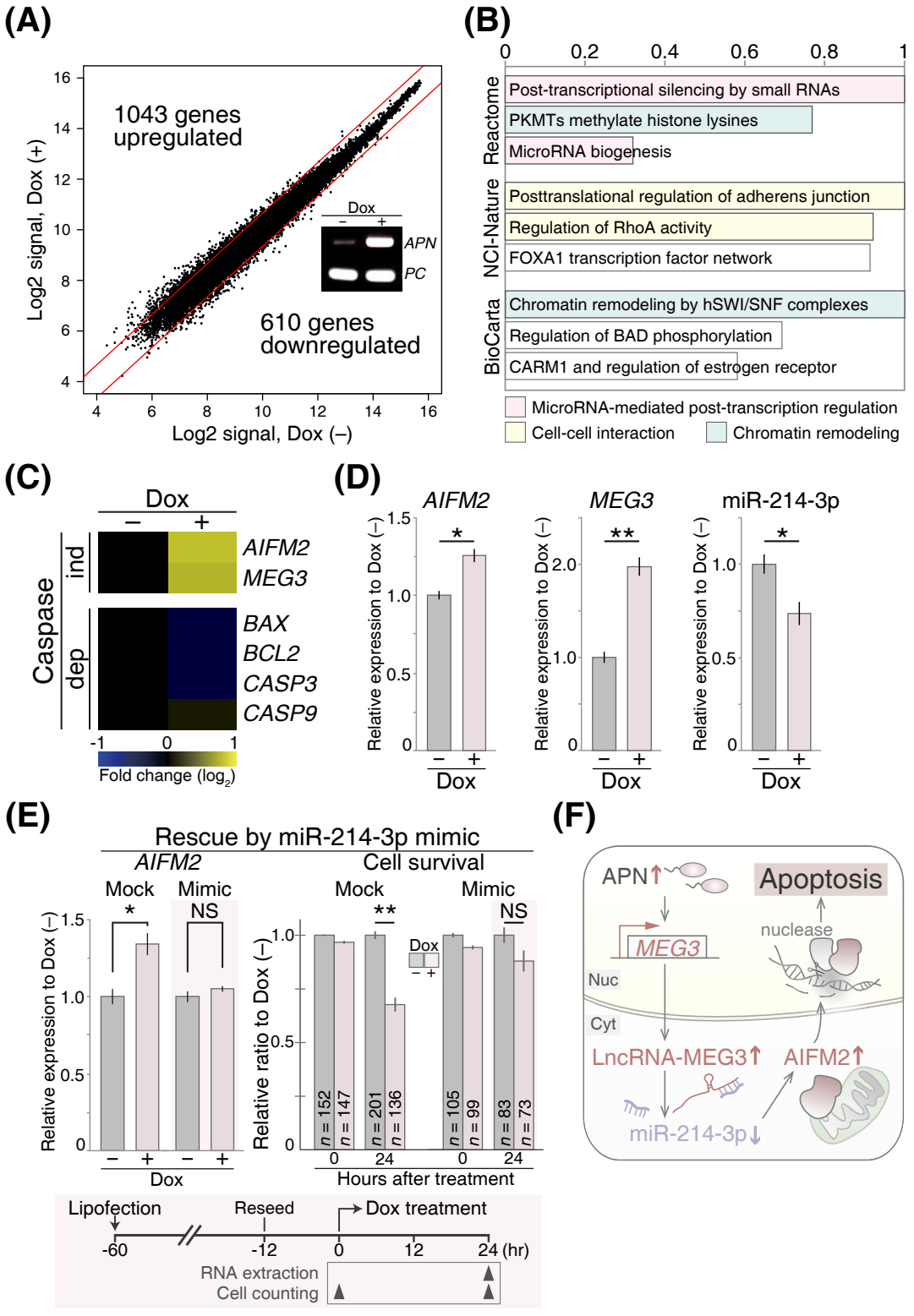
(A)
1043 genes upregulated
610 genes downregulated
Log2 signal, Dox (+)
Log2 signal, Dox (–)
Dox
APN
PC
(B)
Reactome
Post-transcriptional silencing by small RNAs
PKMTs methylate histone lysines
MicroRNA biogenesis
NCI-Nature
Posttranslational regulation of adherens junction
Regulation of RhoA activity
FOXA1 transcription factor network
BioCarta
Chromatin remodeling by hSWI/SNF complexes
Regulation of BAD phosphorylation
CARM1 and regulation of estrogen receptor
MicroRNA-mediated post-transcription regulation
Cell-cell interaction
Chromatin remodeling
(C)
Dox
Caspase
ind
dep
AIFM2
MEG3
BAX
BCL2
CASP3
CASP9
Fold change (log2)
(D)
AIFM2
MEG3
miR-214-3p
Relative expression to Dox (–)
Dox
(E)
Rescue by miR-214-3p mimic
AIFM2
Cell survival
Mock
Mimic
NS
Relative expression to Dox (–)
Relative ratio to Dox (–)
Hours after treatment
Lipofection
Reseed
Dox treatment
RNA extraction
Cell counting
(F)
APN
Apoptosis
MEG3
nuclease
Nuc
Cyt
LncRNA-MEG3
AIFM2
miR-214-3p

Figure 6

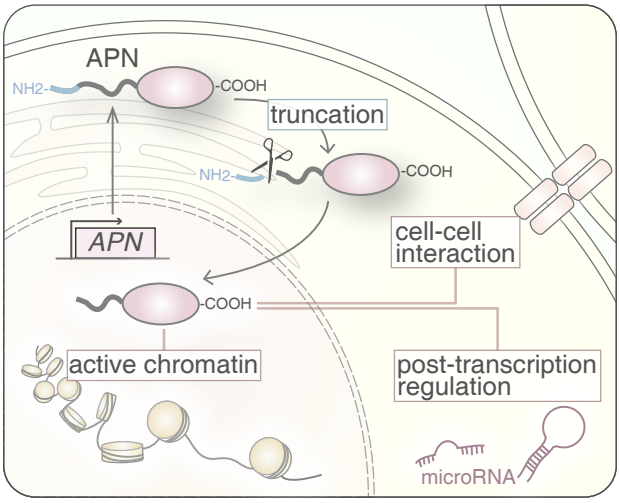
APN
NH2-
-COOH
truncation
NH2-
-COOH
APN
cell-cell
interaction
-COOH
active chromatin
post-transcription
regulation
microRNA

Figure 7

Table S1 Primer sets for PCR in the human and mouse

Gene	5'-Forward-3'	5'-Reverse-3'	Product length (bp)
RT-PCR, qPCR			
Apn	TGTTCCTCTTAATCCTGCCCA	CCAACCTGCACAAGTTCCCTT	104
APN	CCCATTCGCTTTACCAAGAT	CATAGAGTCCATTACGCTCT	292
AIFM2	ATGGTTCGGCTGACCAAGAG	GCCACCACATCATTGGCATC	202
MEG3	CCTGCTGCCCATCTACACCTC	CCTCCTCATCCTTTGCCATCCTGG	116
GAPDH / Gapdh	CTGGCCAAGGTCATCCATGAC	CCATCCACAGTCTTCTGGGTG	92
miRNA qPCR			
miR-214-3p	ACAGCAGGCACAGACAGGCAG	miScript universal primer (QIAGEN)	
miR-214-5p	TGCCTGTCTGTGCCTGCTG	miScript universal primer (QIAGEN)	
DsRed	TACGTGAAGCACCCCGCCGA	GCCGCCGTCCTCGAAGTTCA	96
Plasmid construction			
APN full CDS	GATTCCATACCAGAGGGGCTCAGG	CTGGAGGAGGCTCTGAGTTAGTG	786

bp: base pairs, CDS: coding sequence

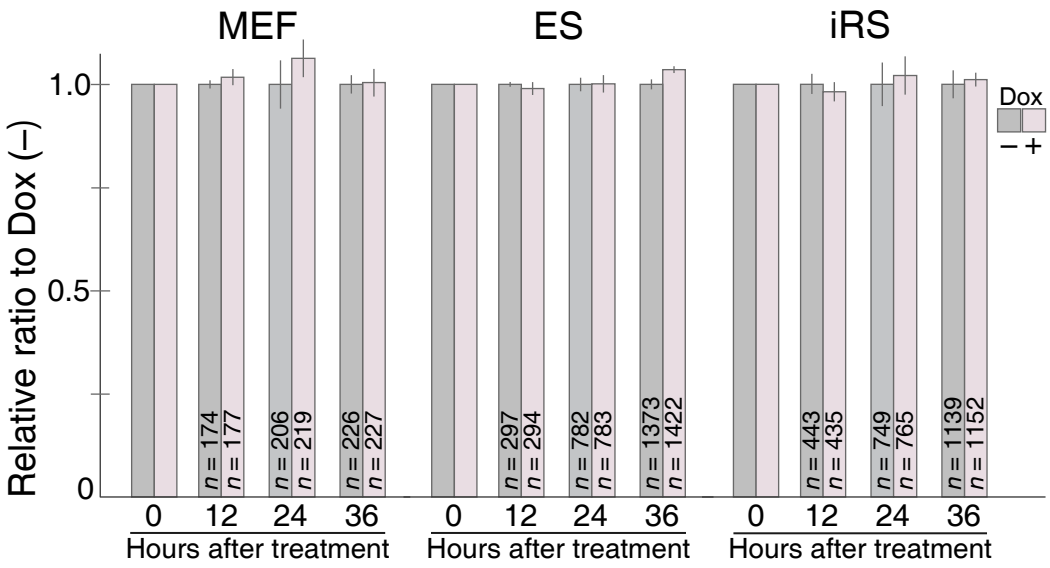

Figure S1. Survival and proliferation of cells in culture in the presence of Doxycycline. The number of cells from three independent experiments was reported as mean ± s.e.m. *n*; the total number of cells counted. MEF; mouse embryonic fibroblasts, ES; mouse embryonic stem cells, iRS; human intermediately reprogrammed stem cells.

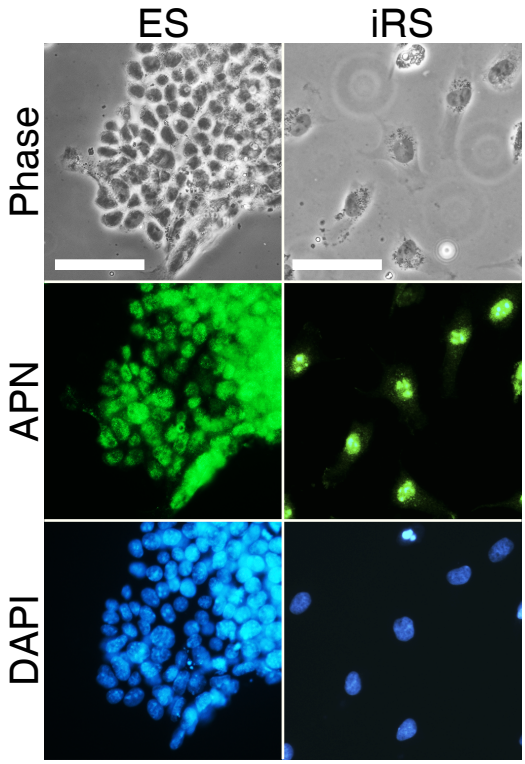

Figure S2. Localization of ADIPONECTIN/Adiponectin protein by immunocytochemistry with an anti-APN/Apn antibody (Ct2). The Ct2 recognized the C-terminal globular domain (Fig. 1A). Apn (green) indicates immunoreactive nuclei, and DAPI (blue) indicates nuclei of pluripotent cells. ES; mouse embryonic stem cells, iRS; human intermediately reprogrammed stem cells. Scale bars: 50 μm.

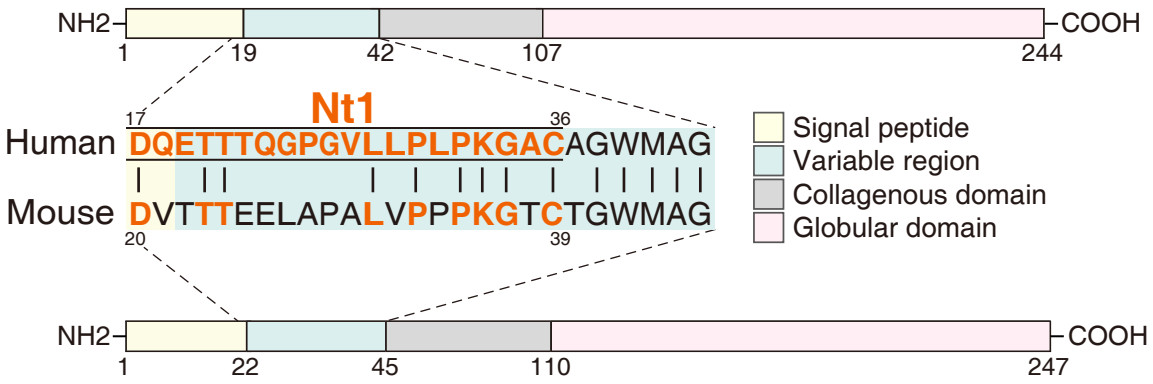

Figure S3. Nt1 recognition site specific to N-terminal variable region of human ADIPONECTIN. The Nt1 antibody recognizes amino acid 17-36 of human ADIPONECTIN (UniProt No. Q15848), which are not similar to amino acid 20-39 (counter part of 17-36 of human) of mouse Adiponectin (UniProt No. Q60994). Orange characters are human amino acids (17-36) recognized by the Nt1 antibody.

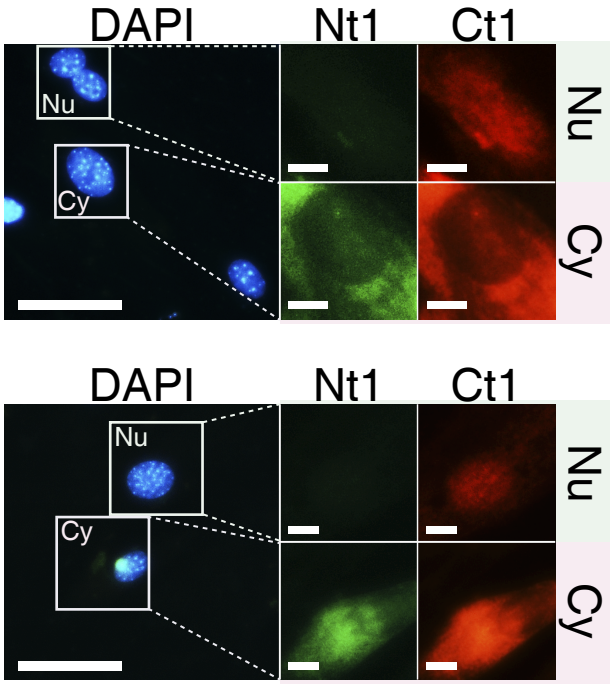

Figure S4. Representative immunocytochemistry of Nt1 to nucleus or cytoplasm-localized human Doxcycline-induced ADIPONECTIN in mouse embryonic fibroblasts (MEFs). Reactivity of Nt1 to human full length ADIPONECTIN is demonstrated in two independently captured images in addition to Figure 5B as a positive control. Nt1, which is specific to human N-terminal ADIPONECTIN, reacts with full length cytoplasm -localized ADIPONECTIN (green), but not N-terminal-truncated nucleus -localized ADIPONECTIN. Ct1, which is specific to human and mouse C-terminal ADIPONECTIN/Adiponectin, reacts both with nucleus-localized truncated and cytoplasm-localized full length ADIPONECTIN/Adiponectin (red). Nt1; N-terminal recognizing antibody (Figure 5A), Ct1; C-terminal recognizing antibody (Figure 5A), Nu; nucleus-localized type, Cy; cytoplasm -localized type. Scale bars: 50 μm in DAPI, and 10 μm in Nt1 and Ct1.

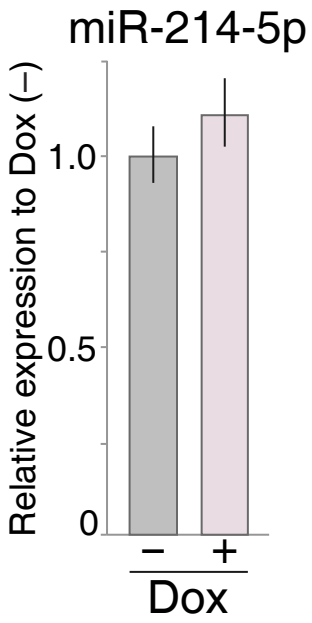

Figure S5. Expression change of miR-214-5p between Dox (-) and Dox (+) by qPCR. Expression levels are presented as the mean ± s.e.m. from five independent experiments.

Laboratory Investigation (2017) 97, 1152–1157

参考論文

MINI REVIEW

Mechanism of human somatic reprogramming to iPS cell

Rika Teshigawara, Junkwon Cho, Masahiro Kameda and Takashi Tada

Somatic reprogramming to induced pluripotent stem cells (iPSC) was realized in the year 2006 in mice, and in 2007 in humans, by transiently forced expression of a combination of exogenous transcription factors. Human and mouse iPSCs are distinctly reprogrammed into a 'primed' and a 'naïve' state, respectively. In the last decade, puzzle pieces of somatic reprogramming have been collected with difficulty. Collectively, dissecting reprogramming events and identification of the hallmark of sequentially activated/silenced genes have revealed mouse somatic reprogramming in fragments, but there is a long way to go toward understanding the molecular mechanisms of human somatic reprogramming, even with developing technologies. Recently, an established human intermediately reprogrammed stem cell (iRSC) line, which has paused reprogramming at the endogenous *OCT4*-negative/exogenous transgene-positive pre-MET (mesenchymal-to-epithelial-transition) stage can resume reprogramming into endogenous *OCT4*-positive iPSCs only by change of culture conditions. Genome-editing-mediated visualization of endogenous *OCT4* activity with GFP in living iRSCs demonstrates the timing of *OCT4* activation and entry to MET in the reprogramming toward iPSCs. Applications of genome-editing technology to pluripotent stem cells will reshape our approaches for exploring molecular mechanisms.
Laboratory Investigation (2017) **97,** 1152–1157; doi:10.1038/labinvest.2017.56; published online 22 May 2017

REPROGRAMMING OF SOMATIC CELLS

Reprogramming somatic cells into induced pluripotent stem cells (iPSCs), which possess unique properties of self-renewal and differentiation into multiple cell lineages, is achieved by transduction using a defined set of transcription factors: Oct4 (Pou5f1), Sox2, Klf4, and c-Myc (OSKM) in mice,[1,2] and humans.[3,4] The success of iPSC generation opens a way to produce patient-specific pluripotent stem cells with less ethical issues than embryonic stem cells (ESCs) generated from fertilized pre-implantation embryos. Personalized iPSCs are expected to contribute to the exploration of cure and cause of diseases, drug screening, and tailor-made regenerative medicine. iPSC generation methodology has improved with different delivery systems, including non-integrating vectors, deletion after integration, DNA-free transduction, and chemical induction.[5–11] Furthermore, novel approaches for iPSC production have been developed, including combinations of alternative transcription factors.[12] In addition to those, reprogramming-susceptible cell types have been identified.[13–15] Even with studious effort for methodological and technical improvements, the efficiency of reprogramming remains ~0.1% in humans, and ~1.0% in mice.[16] Mechanisms of somatic reprogramming have important implications for iPSC applications. Furthermore, iPSCs could be of great use in exploring molecular mechanisms of many diseases and embryonic development as models. However, the low efficiency and stochastic nature of reprogramming hinders the understanding of reprogramming mechanisms.

MECHANISMS OF REPROGRAMMING IN MICE

In mice, the specific order of reprogramming events has been determined as (i) activation of alkaline phosphatase, (ii) silencing of somatic-specific expression, (iii) expression of SSEA1, and (iv) progressive silencing of exogenous genes with concomitant upregulation of endogenous *Oct4* and *Nanog*[17–19] (Figure 1a). *Nanog* is a key player of the stem cell regulatory network critical for acquiring a pluripotent state.[20] EpCAM, c-Kit, and PECAM1 were identified as other surface markers of early, intermediate, and late genes of SSEA1-positive cells, respectively.[21,22] Information on roadblock genes during reprogramming and stage-specific markers for enrichment of intermediately reprogrammed cells prone to forming iPSCs is being accumulated using several advanced technologies.

In addition to the marker genes, pluripotency-associated mmu (Mus Musculus) -microRNAs (miRNAs) are sequentially expressed, and implicated with induction, maturation, and stabilization of unique characteristics of iPSCs[23–25] (Figure 1a). In chromatin reprogramming, pioneer

Department of Developmental Epigenome, Institute for Frontier Life and Medical Sciences, Kyoto University, Kyoto, Japan
Correspondence: Professor T Tada, PhD, Department of Developmental Epigenome, Institute for Frontier Life and Medical Sciences, Kyoto University, 53 Kawahara-cho, Shogoin, Sakyo-ku, Kyoto 606-8507, Japan.
E-mail: ttada@infront.kyoto-u.ac.jp

Received 1 March 2017; revised 10 April 2017; accepted 17 April 2017

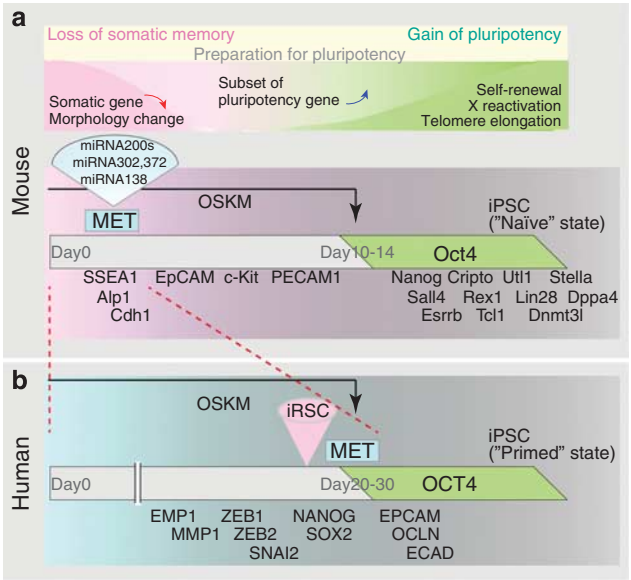

Figure 1 Sequential events, changes of gene and microRNA expression in reprogramming mouse (**a**) and human (**b**) somatic cells to induced pluripotent cells (iPSCs). Mesenchymal-to-epithelial transition (MET) occurs at differential timing in the road of reprogramming. Duration of expression of exogenous reprogramming factors, Oct4, Sox2, Klf4, and c-Myc (OSKM) is indicated by black arrow. Expression of endogenous Oct4/OCT4 is indicated by the green rectangle. Derivation of timing of intermediately reprogrammed stem cells (iRSCs) in the reprogramming process is shown by the pink triangle in humans (**b**).

transcription factors bind directly to condensed chromatin and elicit a series of chromatin remodeling events, including histone modification of H3 lysine 4 and 27 (ref. 26) that lead to opening of chromatin during cell division, which creates opened chromatin situation that other transcription factors are readily accessible.[27] In cell cycle reprogramming, rapid proliferation with a characteristic cell cycle structure of short G1- and G2-gap phases is signature to iPSCs accompanying self-renewal and pluripotency.[28]

MET (mesenchymal-to-epithelial transition), which is the hallmark critical event toward the derivation of iPSCs from mouse embryonic fibroblasts (MEFs), occurs at an early stage of reprogramming.[23,29,30] MET is characterized by upregulation of epithelial genes, *E-Cadherin*, *Cdh1*, *Epcam*, and epithelial-associated mmu-miRNA-200 family, and down-regulation of mesenchymal genes, *Snail1/2*, *Zeb1/2*, and *N-Cadherin*.[31–33] Exogenous Oct4 and Sox2 bind to the promoter regions of mmu-miRNA-141/200c and the mmu-miRNA-200a/b/429 cluster, respectively, and induce transcription activation of the mmu-miRNA-200 family (miRNA-200s).[29]

MET is driven by a strong bone morphogenetic protein (BMP) response through induction of mmu-miRNA-200s and 205 according to the BMP-miRNA-MET pathway.[23] Repression of mmu-miRNA-200s with specific inhibitors results in repression of MET and iPSC generation. Furthermore, the effects of mmu-miRNA-200s and 205 were blocked by *Zeb2* overexpression. Collectively, the mmu-miRNA-200/Zeb2 pathway critically functions in promoting MET at the early stage of somatic reprogramming.[29,34] Moreover, MET is controlled under the orchestrated regulation of epigenetic modification modulated, in part, by H3K36 demethylases Jhdm1a/1b[35] and H3K79 methylase Dot1L.[36] Consequently, MET accompanied by changes in morphology from the somatic to pluripotent type cell induces expression pattern changes in several thousands of genes.[23,24]

MECHANISMS OF REPROGRAMMING IN HUMANS

Human iPSC colonies exhibit characteristic flat-shaped morphology, which is clearly distinct from mouse iPSC colonies that exhibit bowl-shaped morphology. Mouse iPSCs are reprogrammed into a 'naïve' state similar to the state of mouse embryonic stem cells (ESCs), whereas human iPSCs are in a 'primed' state similar to the state of human ESCs, and mouse Epistem cells (EpiSCs)[37,38] (Figure 1b). Mouse ESCs, but not mouse EpiSCs, are germline-competent in blastocyst-injection-mediated chimeras. Notably, 'primed'-state human and 'naïve'-state mouse iPSCs make differential responses in mouse ground state culture conditions with N2B27+2i+LIF medium.[39,40] Distinct pluripotent states between human and mouse iPSCs are also demonstrated by X-chromosome reactivation of female somatic cell reprogramming.[41] Collectively, the final cell fate by somatic reprogramming through forced expression of the same exogenous OSKM transcription factors is distinctive between humans and mice (Figure 1a and b). Thus, it is predicted that parts of the reprogramming process are shared with humans and mice, whereas others are unique to humans or mice.

Indeed, partially diverged interactions of pluripotency-associated miRNAs and the target mRNAs between humans and mice have been summarized.[25] This is consistent with the divergence of sequential reprogramming events between humans and mice. In mice, MET occurs early in reprogramming of MEFs to iPSCs, which precedes the activation of endogenous *Oct4*;[21,23] however, in humans, MET occurs at a later stage of reprogramming with the same timing of endogenous *OCT4* activation (Figures 1a and b). It is likely that MET is a checkpoint for entry into a 'primed' state of pluripotency, whereas activation of an *OCT4/Oct4* is a key step for commitment to further cellular reprogramming through composing OCT4/Oct4-induced pluripotency molecular network. In this context, human iPSCs acquired OCT4-induced pluripotency under a 'primed' state prior to conversion to a 'naïve' state. This implies that, in mice, a 'primed ' state is generated at a much earlier stage, with additional steps required prior to Oct4-induced pluripotency. MET is an event separable from activation of endogenous OCT4/Oct4, as shown by differential timing of entry to MET between human and mouse reprogramming.

The generation of human 'naïve' iPSCs, which demonstrated molecular characteristics and functional properties similar to mouse ESCs/iPSCs, was reported with the

chemically defined culture conditions, NHSM (naïve human stem cell medium).[42] Conversion from a 'primed' state to a 'naïve' state is facilitated by forced expression of exogenous *Klf4* under ground state culture conditions in mice.[43] Furthermore, it was revealed that the pluripotency-associated hsa (Homo sapiens) -miRNA-290/302 family of microRNAs regulates the transition of ESCs from a 'naïve' to 'primed' state of pluripotency.[44] However, in humans, mechanisms involved in 'primed-to-naïve' conversion are largely unknown.

In human ESCs, OCT4, SOX2, and NANOG, which play essential roles in somatic reprogramming to iPSCs, co-occupy a substantial portion of more than 300 target genes with collaboration to form regulatory circuitry consisting of autoregulatory and feedforward loops,[45] suggesting that appropriate transcription of OCT4, SOX2, and NANOG is required to stabilize a pluripotency molecular network for facilitating the maturation of the somatic reprogramming process toward iPSC generation. Prior to stabilization of the pluripotency network through MET and endogenous *OCT4* activation in human reprogrammed cells, a 'primed' pluripotency competent state may be induced by forced expression of *c-Myc* and *Klf4* as demonstrated by mouse reprogramming cells.[30] Recently, several 'naïve'-specific, but not 'primed'-specific, cell surface marker proteins were demonstrated by comprehensive profiling of cell surface proteins by flow cytometry in 'naïve' and 'primed' human pluripotent stem cells (PSCs).[46] It is unclear whether stabilization of human iPSCs under a 'primed' state but not a 'naïve' state resulted from passing through a transient 'naïve' state during reprogramming. Newly identified 'naïve'-specific marker proteins could facilitate to define the human pre-iPSC and iPSC state in the progress of somatic reprogramming.

EXPLORING REPROGRAMMING MECHANISMS WITH AN INTERMEDIATELY REPROGRAMMED STEM CELL LINE

In mice, intermediately reprogrammed cells characterized by silencing somatic genes, activated SSEA1, and the potential of conversion to iPSCs were predicted as a transient cell population, whereas partially reprogrammed cells

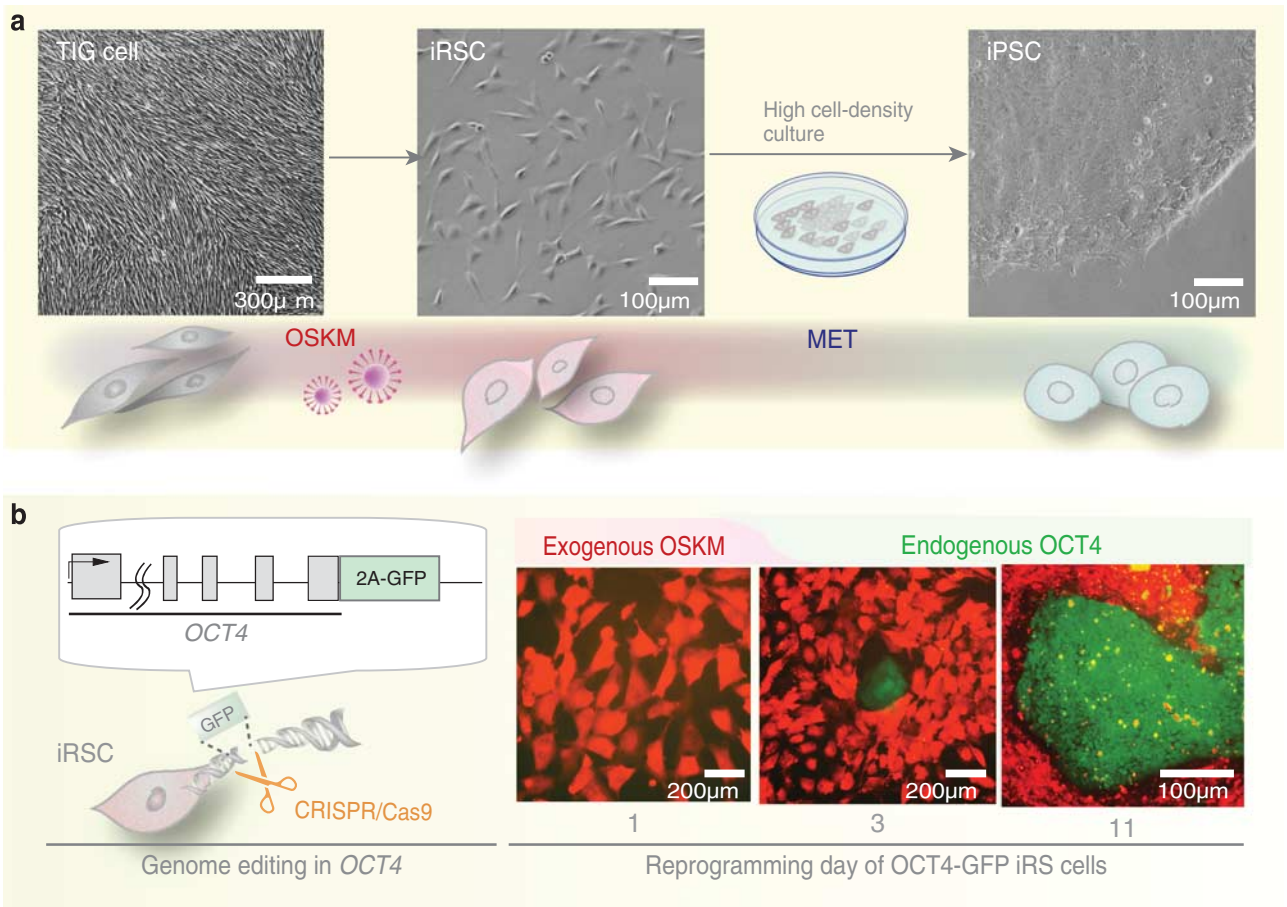

Figure 2 (**a**) Sequential changes of cell morphology from human TIG fibroblast cell, intermediately reprogrammed stem cell (iRSC), to induced pluripotent stem cell (iPSC) in somatic reprogramming. OSKM; reprogramming factor, Oct4, Sox2, Klf4, and c-Myc. (**b**) CRISPR/Cas9-mediated genome editing of the endogenous *OCT4* gene in human iRSCs to visualize the activity of OCT4 by fluorescence marker, GFP (Green Fluorescence Protein) in the reprogramming process of iRSCs to iPSCs. MET; mesenchymal-to-epithelial transition.

characterized by expression of reprogramming transgenes, activated proliferation genes, silencing of pluripotency genes, and aberrant expressing lineage genes were established as several endogenous *Oct4*-negative pre-iPSC lines without potential of conversion to iPSCs.[2,47,48] In humans, partially reprogrammed iPSCs resumed reprogramming by upregulation of *KLF4*,[49] and pre-iPSC-like cell lines were established as cancer stem cell lines.[50] Metabolome profiling demonstrated that human partially reprogrammed iPSCs shared only 74% similarly expressed metabolites with human ESCs,[51] indicating that transcriptome of partially reprogrammed stem cells is considerably different from that of ESCs. Therefore, establishment of iPSC lines makes no promise to establish stable lines of human partially reprogrammed iPSCs. Under such a state, derivation of human intermediately reprogrammed stem cells (iRSCs) as stable lines was unexpected.

Human iRSCs, established from the reprogrammed fetal lung fibroblast cell lines, TIG1 and TIG3, by retroviral transduction of OSKM reprogramming factors were characterized by silencing of somatic genes, activated reprogramming transgenes, self-renewal ability, activated SSEA4, and potential of conversion to iPSCs[52] (Figures 1b and 2a). Notably, iRSCs efficiently resumed the reprogramming process toward iPSC generation under specified culture conditions at a high cell density. Molecular stimuli involved in resuming reprogramming from iRSC to iPSC are elusive. It has been reported that high cell density is a potent negative regulator of cell cycle and expression of genes including retrotransposon,[53] implying that exogenous OSKM genes were silenced as a consequence of high cell densitiy of iRSCs. iRSCs were marked by endogenous expression of core pluripotency factors, *SOX2* and *NANOG* but not *OCT4*, in addition to exogenous OSKM reprogramming factors. Endogenous *OCT4* was activated along with entry to MET and silencing of exogenous transgenes. GFP (green fluorescence protein) knockin to the endogenous *OCT4* locus by CRISPR/Cas9-mediated genome editing-enabled visualization of the *OCT4* activation kinetics in living reprogramming cells transit from iRSCs to iPSCs (Figure 2b). It was revealed that activation of endogenous *OCT4* simultaneously occurring with silencing of exogenous OSKM reprogramming factors is induced prior to entry into MET.

Interestingly, time-lapse analyses of endogenous *OCT4* activity demonstrated that *OCT4*-positive reprogramming cells created *OCT4*-positive and negative daughter cells through asymmetric cell division soon after *OCT4* activation, while *OCT4*-positive cells enabled symmetric cell division to form two daughter cells with the same pluripotent identity in larger growing colonies.[52] It is likely that instability of endogenous *OCT4* is linked to the cell characteristics of symmetric or asymmetric division. It has been debated whether reprogramming entails a hierarchic or stochastic process.[54] Once OSKM factors are silenced and endogenous *OCT4* is activated in a stochastic manner, further reprogramming is proposed to progress in a hierarchical manner.[12] Contrary to this, it was proposed that endogenous *Oct4* activation is insufficient for progression of subsequent events in mouse somatic reprogramming.[55,56] In the maturation process of iRSC-to-iPSC conversion, endogenous *OCT4* activation is essential for iPSC generation, but not sufficient for determining cell fate to be iPSCs.

It is controversial whether the reprogramming pathway from somatic cell to iPSC is a single pathway. This is linked to hypotheses as to whether the reprogramming process occurs in a hierarchic or stochastic manner. It has been proposed, in mice, that the pluripotency spectrum can encompass multiple, unique cell states, including an alternative somatic reprogramming path to iPSCs through a *Nanog*-positive transient state, in addition to the preconceived *Nanog*-negative transient state.[57,58] Collectively, reprogramming mechanisms of cellular reprogramming from somatic cells to iPSCs are more complicated rather than those we expected when OSKM-mediated somatic reprogramming was discovered.

iRSC APPLICATIONS

Understanding of molecular mechanisms involved in human somatic reprogramming will not directly contribute to curing specific diseases of patients, but will be useful for investigating medical biology, including human embryonic development, anti-aging, cell physiology, and epigenetics. To do so, application of genetic manipulation to human iPSCs, which is desirable for repair of genetic mutations and deficiencies, is one of the crucial approaches. Single-cell sub-cloning is an inevitable process for genetic manipulation. However, dissociation-induced pro-apoptosis takes place in subcultures of iPSCs,[59] even using the anti-apoptosis molecule, Rho-associated kinase (ROCK) inhibitor Y-27632.[60] An advantageous property of iRSC use is that they are readily expandable from a single cell after conventional gene modifications. Afterwards, reprogramming from gene-manipulated iRSCs to iPSCs can be feasibly resumed by the change of culture conditions. iRSCs will be a powerful cell source for applying recently developed genome-editing technologies.[61,62] Furthermore, iRSC-based identification of marker genes modulating different reprogramming stages would greatly facilitate the understanding of epigenetic events that occur at each stage by enabling enrichment of subpopulations of reprogramming cells. Integration of a inducible gene expression/repression control system enabled by genetic modifications with iRSCs could help for exploring genes responsible for conversion of iRSCs to 'naïve' iPSCs in the reprogramming. Only a part of the reprogramming mechanism is understood in humans. Further investigation of mechanisms of somatic reprogramming by developing new technologies, and integration with new scientific fields may shed light on the fundamental question of 'what is life'.

ACKNOWLEDGMENTS
We thank Ms Megumi Fukuchi for discussion and help.

DISCLOSURE/CONFLICT OF INTEREST
The authors declare no conflict of interest.

1. Takahashi K, Yamanaka S. Induction of pluripotent stem cells from mouse embryonic and adult fibroblast cultures by defined factors. Cell 2006;126:663–676.
2. Hochedlinger K, Plath K. Epigenetic reprogramming and induced pluripotency. Development 2009;136:509–523.
3. Takahashi K, Okita K, Nakagawa M, *et al.* Induction of pluripotent stem cells from fibroblast cultures. Nat Protoc 2007;2:3081–3089.
4. Lowry WE, Richter L, Yachechko R, *et al.* Generation of human induced pluripotent stem cells from dermal fibroblasts. Proc Natl Acad Sci USA 2008;105:2883–2888.
5. Hussein SM, Nagy AA. Progress made in the reprogramming field: new factors, new strategies and a new outlook. Curr Opin Genet Dev 2012;22:435–443.
6. Zhou H, Wu S, Joo JY, *et al.* Generation of induced pluripotent stem cells using recombinant proteins. Cell Stem Cell 2009;4:381–384.
7. Li X, Zhang P, Wei C, *et al.* Generation of pluripotent stem cells via protein transduction. Int J Dev Biol 2014;58:21–27.
8. Zhou YY, Zeng F. Integration-free methods for generating induced pluripotent stem cells. Genomics Proteomics Bioinformatics 2013;11:284–287.
9. Singh VK, Kumar N, Kalsan M, *et al.* Mechanism of induction: induced pluripotent. J Stem Cells 2015;10:43–62.
10. Schlaeger TM, Daheron L, Brickler TR, *et al.* A comparison of non-integrating reprogramming methods. Nat Biotechnol 2015;33:58–63.
11. Higuchi A, Ling QD, Munusamy MA, *et al.* Generation of pluripotent stem cells without the use of genetic material. Lab Invest 2015;95:26–42.
12. Buganim Y, Faddah DA, Cheng AW, *et al.* Single-cell expression analyses during cellular reprogramming reveal an early stochastic and a late hierarchic phase. Cell 2012;150:1209–1222.
13. Wernig M, Zhao JP, Pruszak J, *et al.* Neurons derived from reprogrammed fibroblasts functionally integrate into the fetal brain and improve symptoms of rats with Parkinson's disease. Proc Natl Acad Sci USA 2008;105:5856–5861.
14. Nagata S, Toyoda M, Yamaguchi S, *et al.* Efficient reprogramming of human and mouse primary extra-embryonic cells to pluripotent stem cells. Genes Cells 2009;14:1395–1404.
15. Polo JM, Liu S, Figueroa ME, *et al.* Cell type of origin influences the molecular and functional properties of mouse induced pluripotent stem cells. Nat Biotechnol 2010;28:848–855.
16. Stadtfeld M, Hochedlinger K. Induced pluripotency: history, mechanisms, and applications. Genes Dev 2010;24:2239–2263.
17. Brambrink T, Foreman R, Welstead GG, *et al.* Sequential expression of pluripotency markers during direct reprogramming of mouse somatic cells. Cell Stem Cell 2008;2:151–159.
18. Stadtfeld M, Maherali N, Breault DT, *et al.* Defining molecular cornerstones during fibroblast to iPS cell reprogramming in mouse. Cell Stem Cell 2008;2:230–240.
19. David L, Polo JM. Phases of reprogramming. Stem Cell Res 2014;12:754–761.
20. Silva J, Nichols J, Theunissen TW, *et al.* Nanog is the gateway to the pluripotent ground state. Cell 2009;138:722–737.
21. Polo JM, Anderssen E, Walsh RM, *et al.* A molecular roadmap of reprogramming somatic cells into iPS cells. Cell 2012;151:1617–1632.
22. Nefzger CM, Alaei S, Knaupp AS *et al.* Cell surface marker mediated purification of iPS cell intermediates from a reprogrammable mouse model. J Vis Exp 2014;91:e51728.
23. Samavarchi-Tehrani P, Golipour A, David L, *et al.* Functional genomics reveals a BMP-driven mesenchymal-to-epithelial transition in the initiation of somatic cell reprogramming. Cell Stem Cell 2010;7:64–77.
24. Esteban MA, Boa X, Zhuang Q, *et al.* The mesenchymal-to-epithelial transition in somatic cell reprogramming. Curr Opin Genet Dev 2012;22:423–428.
25. Leonardo TR, Schultheisz HL, Loring JF, *et al.* The functions of microRNAs in pluripotency and reprogramming. Nat Cell Biol 2012;14:1114–1121.
26. Park J, Kwon YW, Ham S, *et al.* Identification of the early and late responder genes during the generation of induced pluripotent stem cells from mouse fibroblasts. PLoS ONE 2017;12:e0171300.
27. Krause MN, Sancho-Martinez I, Izpisua Belmonte JC. Understanding the molecular mechanisms of reprogramming. Biochem Biophys Res Commun 2016;473:693–697.
28. Boward B, Wu T, Dalton S. Concise review: control of cell fate through cell cycle and pluripotency networks. Stem Cells 2016;34:1427–1436.
29. Wang G, Guo X, Hong W, *et al.* Critical regulation of miR-200/ZEB2 pathway in Oct4/Sox2-induced mesenchymal-to-epithelial transition and induced pluripotent stem cell generation. Proc Natl Acad Sci USA 2013;110:2858–2863.
30. Li R, Liang J, Ni S, *et al.* A mesenchymal-to-epithelial transition initiates and is required for the nuclear reprogramming of mouse fibroblasts. Cell Stem Cell 2010;7:51–63.
31. Mikkelsen TS, Hanna J, Zhang X, *et al.* Dissecting direct reprogramming through integrative genomic analysis. Nature 2008;454:49–55.
32. Sridharan R, Plath K. Illuminating the black box of reprogramming. Cell Stem Cell 2008;2:295–297.
33. Polo JM, Hochedlinger K. When fibroblasts MET iPSCs. Cell Stem Cell 2010;7:5–6.
34. Lamouille S, Subramanyam D, Blelloch R, *et al.* Regulation of epithelial-mesenchymal and mesenchymal-epithelial transitions by microRNAs. Curr Opin Cell Biol 2013;25:200–207.
35. Wang T, Chen K, Zeng X, *et al.* The histone demethylases Jhdm1a/1b enhance somatic cell reprogramming in a vitamin-C-dependent manner. Cell Stem Cell 2011;9:575–587.
36. Onder TT, Kara N, Cherry A, *et al.* Chromatin-modifying enzymes as modulators of reprogramming. Nature 2012;483:598–602.
37. Chia NY, Chan YS, Feng B, *et al.* A genome-wide RNAi screen reveals determinants of human embryonic stem cell identity. Nature 2010;468:316–320.
38. Hanna J, Cheng AW, Saha K, *et al.* Human embryonic stem cells with biological and epigenetic characteristics similar to those of mouse ESCs. Proc Natl Acad Sci USA 2010;107:9222–9227.
39. Ying QL, Wray J, Nichols J, *et al.* The ground state of embryonic stem cell self-renewal. Nature 2008;453:519–523.
40. Hirano K, Nagata S, Yamaguchi S, *et al.* Human and mouse induced pluripotent stem cells are differentially reprogrammed in response to kinase inhibitors. Stem Cells Dev 2012;21:1287–1298.
41. Pasque V, Plath K. X chromosome reactivation in reprogramming and in development. Curr Opin Cell Biol 2015;37:75–83.
42. Gafni O, Weinberger L, Mansour AA, *et al.* Derivation of novel human ground state naive pluripotent stem cells. Nature 2013;504:282–286.
43. Guo G, Yang J, Nichols J, *et al.* Klf4 reverts developmentally programmed restriction of ground state pluripotency. Development 2009;136:1063–1069.
44. Gu KL, Zhang Q, Yan Y, *et al.* Pluripotency-associated miR-290/302 family of microRNAs promote the dismantling of naive pluripotency. Cell Res 2016;26:350–366.
45. Boyer LA, Lee TI, Cole MF, *et al.* Core transcriptional regulatory circuitry in human embryonic stem cells. Cell 2005;122:947–956.
46. Collier AJ, Panula SP, Schell JP *et al.* Comprehensive cell surface protein profiling identifies specific markers of human naive and primed pluripotent states. Cell Stem Cell 2017. e-pub ahead of print 21 March 2017; doi: 10.1016/j.stem.2017.02.014.
47. Theunissen TW, Van Oosten AL, Castelo-Branco G, *et al.* Nanog overcomes reprogramming barriers and induces pluripotency in minimal conditions. Curr Biol 2011;21:65–71.
48. Chen J, Liu H, Liu J, *et al.* H3K9 methylation is a barrier during somatic cell reprogramming into iPSCs. Nat Genet 2013;45:34–42.
49. Nishimura K, Kato T, Chen C, *et al.* Manipulation of KLF4 expression generates iPSCs paused at successive stages of reprogramming. Stem Cell Rep 2014;3:915–929.
50. Nagata S, Hirano K, Kanemori M, *et al.* Self-renewal and pluripotency acquired through somatic reprogramming to human cancer stem cells. PLoS ONE 2012;7:e48699.

51. Park SJ, Lee SA, Prasain N, *et al.* Metabolome profiling of partial and fully reprogrammed induced pluripotent stem cells. Stem Cells Dev 2017; doi:10.1089/Scd.2016.0320.
52. Teshigawara R, Hirano K, Nagata S, *et al.* OCT4 activity during conversion of human intermediately reprogrammed stem cells to iPSCs through mesenchymal-epithelial transition. Development 2016;143:15–23.
53. Frisa PS, Jacobberger JW. Cell density related gene expression: SV40 large T antigen levels in immortalized astrocyte lines. BMC Cell Biol 2002;3:10.
54. Yamanaka S. Elite and stochastic models for induced pluripotent stem cell generation. Nature 2009;460:49–52.
55. Greder LV, Gupta S, Li S, *et al.* Analysis of endogenous Oct4 activation during induced pluripotent stem cell reprogramming using an inducible Oct4 lineage label. Stem Cells 2012;30:2596–2601.
56. Silva J, Barrandon O, Nichols J, *et al.* Promotion of reprogramming to ground state pluripotency by signal inhibition. PLoS Biol 2008;6:e253.
57. Tonge PD, Corso AJ, Monetti C, *et al.* Divergent reprogramming routes lead to alternative stem-cell states. Nature 2014;516: 192–197.
58. Jackson SA, Olufs ZP, Tran KA, *et al.* Alternative routes to induced pluripotent stem cells revealed by reprogramming of the neural lineage. Stem Cell Rep 2016;6:302–311.
59. Ohgushi M, Sasai Y. Lonely death dance of human pluripotent stem cells: ROCKing between metastable cell states. Trends Cell Biol 2011;21: 274–282.
60. Watanabe K, Ueno M, Kamiya D, *et al.* A ROCK inhibitor permits survival of dissociated human embryonic stem cells. Nat Biotechnol 2007;25: 681–686.
61. Hockemeyer D, Jaenisch R. Induced pluripotent stem cells meet genome editing. Cell Stem Cell 2016;18:573–586.
62. Waddington SN, Privolizzi R, Karda R, *et al.* A Broad overview and review of CRISPR-Cas technology and stem cells. Curr Stem Cell Rep 2016;2:9–20.